The sea ice in Young Sound: Implications for carbon cycling

Ronnie N. Glud[1], Søren Rysgaard[2], Michael Kühl[1] and Jens W. Hansen[3]

[1] Marine Biological Laboratory, University of Copenhagen, Strandpromenaden 5, DK-3000 Helsingør, Denmark
[2] Greenland Institute of Natural Resources, Kivioq 2, Box 570, DK-3900 Nuuk, Greenland
[3] National Environmental Research Institute, Vejlsøvej 25, DK-8600 Silkeborg, Denmark

Abstract

Most of the year, Young Sound is covered by c. 160 cm thick sea ice overlain by a 20-100 cm thick snow cover. During the last 50 years the sea-ice-free period has varied between 63 and 131 days, but during the last 10–15 years there has been a tendency towards an increase in the sea-ice-free period, and 7 of the longest sea-ice-free periods observed in 50 years were recorded after 1990. The snow and sea-ice cover regulates the activity of the light-limited marine ecosystem of Young Sound. As the snow cover melts during late May and June, the irradiance reflectance decreases, especially for red and near infrared light. Differences in snow cover thickness and patchy distribution of dry snow, wet snow and melting ponds on the sea-ice surface result in a very heterogeneous light environment at the underside of the ice. In areas with sufficient light, sea-ice algae begin to flourish on the available nutrients. The sea-ice algal community adapts efficiently to the local light environment, and in areas with natural (or man-made) holes and cracks sea-ice algae bloom. However, despite ample nutrients, the overall phototrophic biomass in Young Sound remains very low, with maximum values of c. 15–30 µg Chl a l^{-1} sea ice at the underside of the ice and with maximum area integrated values of c. 3 mg Chl a m^{-2}. We speculate that the extreme dynamics in sea-ice appearance, structure and brine percolation, which is driven primarily by large but variable freshwater inputs during snow melt and the breaking of frozen rivers, transforms the sea-ice matrix into a hostile environment for sea-ice algae. An annual estimate of sea-ice-related gross primary production for the entire outer Young Sound (Region 1 c. 76 km^2) amounted to only 2.7 t C. The primary production measurements were performed in 1999 and 2002, and we cannot exclude large inter annual variations. However, we have not experienced massive blooming of sea-ice algae in Young Sound during the last decade.

Detailed *in situ* and laboratory-based microsensor investigations documented that O_2 concentrations at the underside of the ice and within the sea-ice matrix were extremely dynamic and strongly regulated by physical processes related to freezing and thawing of sea water rather than biological activity. Enclosure experiments on sea-ice samples performed in June 2002 revealed a high heterotrophic potential causing the sea-ice environment to become anoxic within 8 days despite concurrent photosynthetic activity. The sea ice was thus net heterotrophic, at least intermittently, and the sea ice hosted a bacterial community of denitrifiers. These findings change our conceptual and quantitative understanding of sea-ice-related microbial activity - at least in settings similar to Young Sound.

4.1 Introduction

Sea-ice cover greatly affects element cycling and regulates primary production in polar environments. During ice cover, the propagation of light to the underside of the ice is strongly impeded due to strong backscattering and attenuation, primarily in the snow cover but also within the sea-ice matrix. This is reflected in a positive correlation between annual primary production and the length of the open-water period in polar and sub-polar regions (Rysgaard et al., 1999). A significant fraction of the light-limited

aquatic primary production in polar ecosystems can be associated with the sea-ice rather than with the pelagic or benthic environments (Horner & Schrader, 1982; Palmisano & Sullivan, 1983; Gosselin et al., 1997; McMinn et al., 2000). Sea-ice algae primarily flourish at the water-ice interface, but algae encrusted inside the ice matrix experience higher light levels and can contribute significantly to the total sea-ice-related primary production (Mock & Gradinger 1999).

The sea-ice algae represent a food source for metazoan grazers (Grainger & Mohammed, 1990; Gradinger & Spindler, 1999) and leakage of photosynthetic products or entrapped organic material can lead to elevated bacterial abundances within the sea ice (e.g. Gradinger & Zhang, 1997; Gradinger & Ikävalko, 1998; Giannelli et al., 2001; Meiners et al., 2003). The sea-ice biota consists of a complete food web with primary and secondary production, a microbial loop and three to four trophic levels (e.g. Horner et al., 1992; Schnack-Schiel et al., 2001). Sea-ice-related processes interact with the underlying water via ice melting/freezing, advection and grazing. In order to quantify and understand polar carbon cycling, it is therefore of prime importance to include the sea-ice-related activity.

During freezing of seawater, crystals of low-salinity water form while dissolved salts and gases freeze out, forming brine inclusions and gas bubbles within the sea-ice matrix. In contrast to freshwater ice, sea ice is thus permeated with pores and brine channels that form more or less interconnected networks in the matrix of solid ice crystals (e.g. Eicken, 2003). The total pore volume of sea ice typically ranges between 1 and 20% depending on temperature, salinity and ionic composition of the brine fluid (Weeks & Ackley, 1986). At decreasing temperatures the thermodynamic phase equilibrium drives the sea ice towards a lower pore space volume and towards increasing brine salinity. Thus, winter sea ice exposed to temperatures below -20ºC contains less than 1% pore space with brine salinity levels well above 200 (Cox & Weeks 1983). The lower part of the sea ice close to the water phase is, however, kept near the freezing point of sea water (c. -1.8ºC) and is thus more permeable than the upper layers of the sea ice. The individual brine inclusions vary in size from a few micrometers to several centimeters (Weissenberger et al., 1992; Golden et al., 1998), and sea-ice thus contains a variety of enclosed and semi-enclosed microniches exhibiting a variety of environmental conditions and harboring different biota and microbial activities. The degree of interconnection of the brine enclosures generally increases with temperature and the potential for percolation of brine through the sea-ice matrix therefore increases towards the polar spring (Eicken et al., 2000). The sea-ice matrix is thus highly heterogeneous, dynamic and difficult to access by standard measuring techniques, and quantification of *in situ* biogeochemical activities in sea ice represents a true challenge to any experimentalist.

A complete study on sea-ice dynamics and the associated biota requires a multidisciplinary approach involving a number of different scientific fields, and many components need careful attention. Our work on sea ice in Young Sound does not provide a complete and exhaustive investigation of the sea ice in the area, but rather a focused effort resolving light conditions, nutrient and gas dynamics, primary production and, to a lesser extent, heterotrophic activity in order to provide estimates on the quantitative importance of sea ice for the local carbon cycling. Most of the presented data were collected during two field campaigns performed from 7 June–5 July 1999 and 28 May–12 June 2002.

4.2   Methods

A number of different techniques were applied during the study. Most of these represent standard measuring routines for sea-ice studies and will not be dealt with in any detail here. For further information on these techniques please refer to the literature. However, we developed and applied *in situ* instruments that are not widely used, and these are described in some detail below.

4.2.1 Sampling and basic routine measurements
Unless anything else is specified the presented measurements were obtained in close vicinity to Station A at 74°18N, 20°15W in outer Region 1 (Chapter 3). Intact sea-ice cores (9 cm id.) were sampled by a MARK II coring system (Kovacs Enterprises, Lebanon, NH , USA). Temperature profiles were measured immediately after recovery by placing solid digital thermosensors in holes of 3 mm in diameter drilled to the center of the core. Intact sections of sea ice were completely thawed for determination of bulk salinity
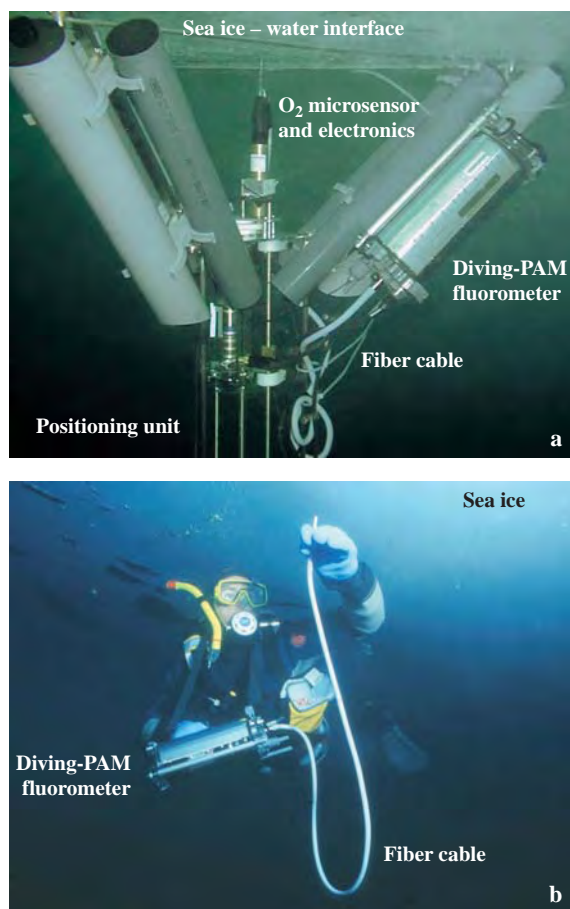
Figure 4.1 (a) The microprofiling instrument placed at the underside of the ice. The central torpedo carrying the microelectrode contains the measuring circuit and is connected to the upper sea-ice surface via a cable. The diving PAM fluorometer is mounted on one of the tripod legs. When fluorescent signals were measured via the tripod, the tip of the fiber cable was mounted on the central "torpedo". **(b)** Diver-operated PAM fluorometer used for estimating phototrophic biomass and photosynthetic activity at the underside of the ice. Photos from Rysgaard et al. (2001).

and nutrient concentrations. Brine concentrations were calculated using the equations of Cox & Weeks (1983) and Leppäranta & Manninen (1988). Samples for nutrient analysis were filtered through GF/F filters and frozen at -18°C until further analysis, while the filters were extracted for 24 h in 96% ethanol and analyzed on a fluorometer for Chl *a* (Jespersen and Christoffersen 1987). Salinity was quantified with a calibrated conductivity meter (Knick, Germany). Concentrations of NO_3^- and NO_2^- were determined as described by Braman & Hendrix (1989), and NH_4^+ concentrations were measured according to Bower & Holm-Hansen (1980). Phosphate concentrations were determined

spectrophotometrically (Grasshoff et al., 1983). Dissolved organic carbon (DOC) was determined with a Shimadzu DOC-5000 Analyzer on melted sea-ice samples after filtration (combusted GF/F filters).

For determination of the gas bubble volume in the sea ice, sections of preweighed ice samples were placed in artificial seawater in 200-ml gas tight glass syringes fitted with 50-cm transparent *Tygon* tubes (id. 3mm). After thawing (at +2°C) the volume of the accumulated gas bubble was determined by pushing it into the tube and measuring the length of the bubble. The oxygen content of the thawed sea-ice sample and the gas bubble was determined by Winkler titration and GC analysis, respectively, and from these data the total O_2 concentration of sea ice samples was calculated according to Rysgaard & Glud (2004).

Sea-ice-related primary production was estimated in sections of the intact sea-ice cores or on sea-ice samples collected by divers from the underside of the ice. The samples were crushed, homogenized and mixed with GF/F-filtered seawater and subsequently incubated with ^{14}C-labeled DIC in glass bottles placed below the sea ice for approximately 2 h (Steemann-Nielsen, 1958; Rysgaard et al., 2001). The ^{14}C fixation was corrected for unspecific labeling measured in dark-incubated bottles and primary production rates were quantified as described by Rysgaard et al. (2001). Denitrification and anaerobic ammonium oxidation (*anammox*) rates in thawed sea-ice were measured by incubating samples with various combinations of $^{15}NO_3^-$, $^{15}NH_4^+$ and $^{14}NO_3^-$ (for details, see Rysgaard & Glud, 2004).

4.2.2 *In situ* microprofile measurements

The biological activity in sea ice is commonly inferred from measurements performed on thawed and homogenized samples. Consequently, the micro-environment (temperature, salinity, nutrient concentrations etc.) of the sea ice has been dramatically changed and the original activity of the sample is no longer preserved. In order to circumvent these problems we constructed a special microprofiling instrument capable of measuring *in situ* O_2 microprofiles at the ice-water interface (Fig. 4.1a). With this instrument it was our aim to obtain *in situ* information about net photosynthesis and aerobic respiration in the lowermost layer of the intact sea ice.

Clark-type oxygen microelectrodes (Revsbech, 1989) were mounted directly on a torpedo-shaped

cylinder containing a custom-made picoamperemeter (Unisense A/S, Denmark). The sensors had tip diameters of 50–150 μm, a stirring sensitivity <2% and a t_{90} response time <2 s (Glud et al., 2000). The measuring system was mounted on a motor-driven spindle fastened to a metal tripod allowing vertical positioning of the sensor tip. Signal recording and motor control was achieved via a 50 m long underwater cable connected to a controller box at the sea ice surface. Sensor calibration was performed during deployment at *in situ* temperature and salinity by exposing the sensor to anoxic and 100% air-saturated water samples. Divers carefully placed the tripod at the underside of the sea ice (avoiding local disturbance and trapping of air bubbles at the measuring site) and the positive buoyancy of air-filled tubes kept the tripod in place during measurements (Kühl et al., 2001; Rysgaard et al., 2001). The O_2 distribution across the water-ice interface was subsequently measured *in situ* under ambient flow and light conditions.

4.2.3 *In situ* Pulse Amplitude Modulated (PAM) fluorometer measurements

Proxies for microalgal biomass (F_0) and photosynthetic activity (rel. ETR) at the underside of the sea ice were measured *in situ* using a pulse amplitude modulation fluorometer (Diving-PAM, Walz GmbH, Germany). A detailed description of the measuring scheme and its application on sea ice can be found in Kühl at al. (2001) and Rysgaard et al. (2001). In short, a 1 m long (8 mm outer diameter) fiber cable guided probing light, actinic light and the variable fluorescence signals between the waterproof fluorometer and the measuring spot. A SCUBA-diver probed various sites in pre-defined grids below the sea ice (Fig. 4.1b). For longer-term measurements the fiber tip was mounted on the moving axis of the tripod described above (Fig. 4.1a).

The apparent minimal fluorescence at the measuring spots, F_0 (which is not the true F_0 value as it was impossible to completely dark adapt the spots due to midnight sun), was obtained by exposing spots with modulated non-actinic levels of probing light emitted by the integrated blue LED in the fluorometer (Schreiber et al., 1986). In order to convert the fluorescence signals into photosynthetic biomass, calibrations were performed on sea-ice-encrusted microalgal cultures with a known Chl *a* content (Rysgaard et al., 2001; Glud et al., 2002). In the applied

configuration the detection limit amounted to c. 0.3 μg C l^{-1}.

The relative electron transport rate (rel. ETR) between photosystems II and I of algae inhabiting the lowermost surface of the sea ice was determined by Diving-PAM using the so-called saturation pulse method (Schreiber et al., 1995; Kühl et al., 2001). The effective quantum yield of PSII-related photosynthetic electron transport was measured at increasing levels of actinic light from a halogen lamp integrated in the Diving-PAM. The actinic light levels were determined with a Licor underwater irradiance meter. Relative electron transport rates, used here as a proxy for the relative photosynthetic rate, were calculated at each experimental irradiance as the product of effective quantum yield (ϕ_d) and the amount of actinic light. In this way, curves of rel. ETR vs. irradiance could be measured *in situ*, yielding information on photosynthetic performance and light acclimation of sea ice algae under natural conditions.

4.3 Results & discussion

4.3.1 Seasonal and interannual variation in ice cover

During the last decades, the sea-ice cover in Young Sound has typically established itself around the end of September. Initially, the sea-ice thickness increases by approximately 2 cm d^{-1}, a rate that gradually decreases to <0.5 cm d^{-1} in January to March. The maximum sea-ice thickness of 140-160 cm is usually reached in April and by then the sea ice surface is covered by a snow layer of variable thickness (20-100 cm). The snow cover strongly affects the light conditions below and within the sea ice and drifting snow introduces a marked patchiness in light distribution at the underside of the sea-ice. The sea-ice cover is hinged to the shore and mechanical stress induced by tidal variations forms cracks and patches of open water that gradually broaden and expand along the shore lines during May–June. The melting of the sea ice accelerates during June–July until the 30–120 cm thick sea-ice cover is exported to the Greenland Sea by wind or current-induced forcing on the now free-floating ice-floes. This breakup of sea ice typically occurs in mid-July (Fig. 4.2). The ice cover of Young Sound is thus characterized as fast ice (first-year sea ice) and older floes from the pack ice in the Greenland Sea are seldom trapped within the fjord.
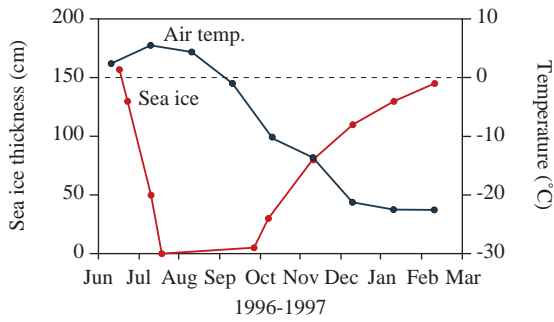
Figure 4.2 Air temperature and sea-ice thickness during 1996–1997. The data reflect the typical seasonality as experienced in Young Sound during the last decades. Data from Rysgaard et al. (1998).

The total sea-ice thickness typically remains in quasi-steady state during April to early June. During this period the sea-ice environment becomes extremely dynamic. Elevated air-temperatures lead to snow melting and the formation of a freshwater layer on top of the sea ice. During periods of colder weather, this can lead to the formation of a secondary ice layer whereby a lens of freshwater separates the thick sea ice from a thinner layer of freshwater ice below the gradually melting snow cover (Fig. 4.3). Temperature variations, tidal movements and wind-induced forcing along with macroscopic cracks and breathing holes of marine mammals can lead to periodic freshwater percolation through the sea-ice matrix. This becomes especially apparent at the bottom of

Figure 4.3 A schematic vertical profile through the snow/sea-ice cover reflecting conditions in Young Sound during the period mid-May–mid June.
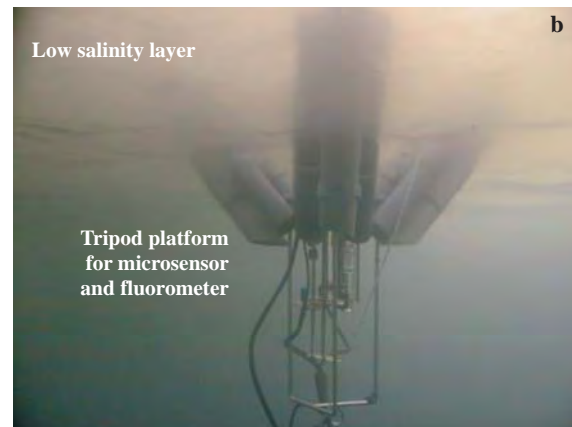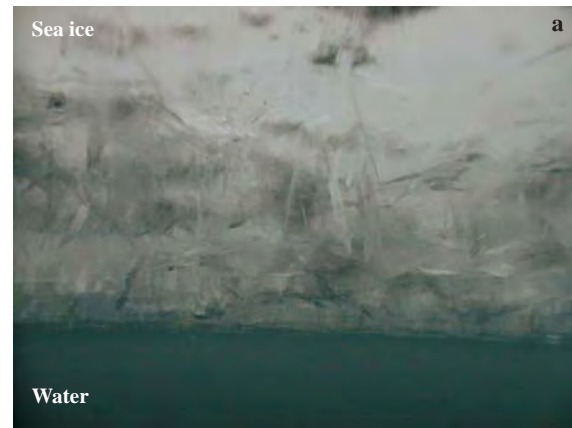
Figure 4.4 Photos of the underside of the sea ice on 14 June 1999 **(a)** and 2 July 1999 **(b)**. Together with Fig. 1a, (obtained 13 June the same year), the photos document the extreme variability in appearance of the underside of the ice during this period. Photos from Rysgaard et al. (2001).

the sea ice, where the appearance can change in a few hours from a solid homogenous surface to a spongy and highly heterogeneous structure with a topography characterized by long, spiny ice crystals, which form when meltwater from above encounters the sub-zero temperatures in the sea water below (Fig. 4.4a). Temperature changes in the surface water or strong tidal flows can reestablish the original hard and homogenous sea ice as the spiny structures melt or are eroded away mechanically. When a larger amount of freshwater is introduced suddenly to the bottom of the sea-ice, a large lens of low-salinity water is established. This becomes very extensive when the rivers of the area break and release millions of m³ of freshwater into the fjord (Fig. 4.4b, see Chapter 2). The massive freshwater input has large consequences for the sea-ice environment and the associated biological activity (see below), and the dynamic behavior of the sea-ice structure during that period constantly frustrated our attempts to quantify the biogeochemical activity of the system.

During the short ice-free period, ice floes or icebergs occasionally enter Young Sound and drift around in a circular pattern in the outer fjord system until they are re-exported to the Greenland Sea (see Chapter 3). This occasional re-entry of ice into Young Sound during the "open-water" period probably has no impact on the larger-scale carbon cycling of the area. Young Sound is thus typically ice covered for 9–10 months of the year. However, the interannual variation is considerable, and during the last 50 years the ice-free period has varied between 63 and 131 days. Especially during the last few years the open-water period has been exceptionally long, and over the last decades a trend towards an extended open-water period is apparent (Fig. 4.5). The prolonged

open-water period in Young Sound complies with observations of increasing temperatures and generally decreasing sea-ice cover in the Greenland Sea.

4.3.2 Reflection, extinction coefficients and light spectra of the sea ice

The snow and sea-ice cover regulates the availability of light for aquatic primary production. Thus, basic information on snow and sea-ice reflectance and light attenuation is essential for a quantitative assessment of local carbon cycling. Generally, the optics of snow and sea ice is well studied (Perovich, 1996 and references therein) and several radiative transfer models have been formulated (e.g. Perovich, 2003). However, our aim with the light measurements in the present study was to obtain important background data on irradiance rather than a detailed optical characterization of the sea ice. Thus, instead of exhaustive optical measurements or the use of radiative transfer models for sea ice (Perovich, 2003), we performed a limited number of irradiance measurements with
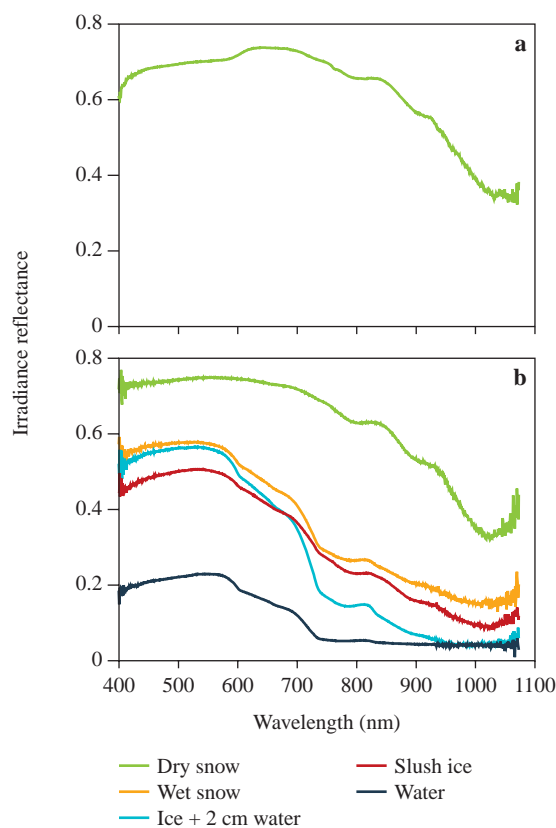
Figure 4.6 The irradiance reflectance (downwelling/upwelling irradiance) measured in different snow types around Station A on 10 and 29 June before and during melting, respectively (Figs. a and b).

Figure 4.5 The number of ice-free days in Young Sound during the last 50 years. Most data are extracted from the logbook of the military patrol, SIRIUS, operating in the area.
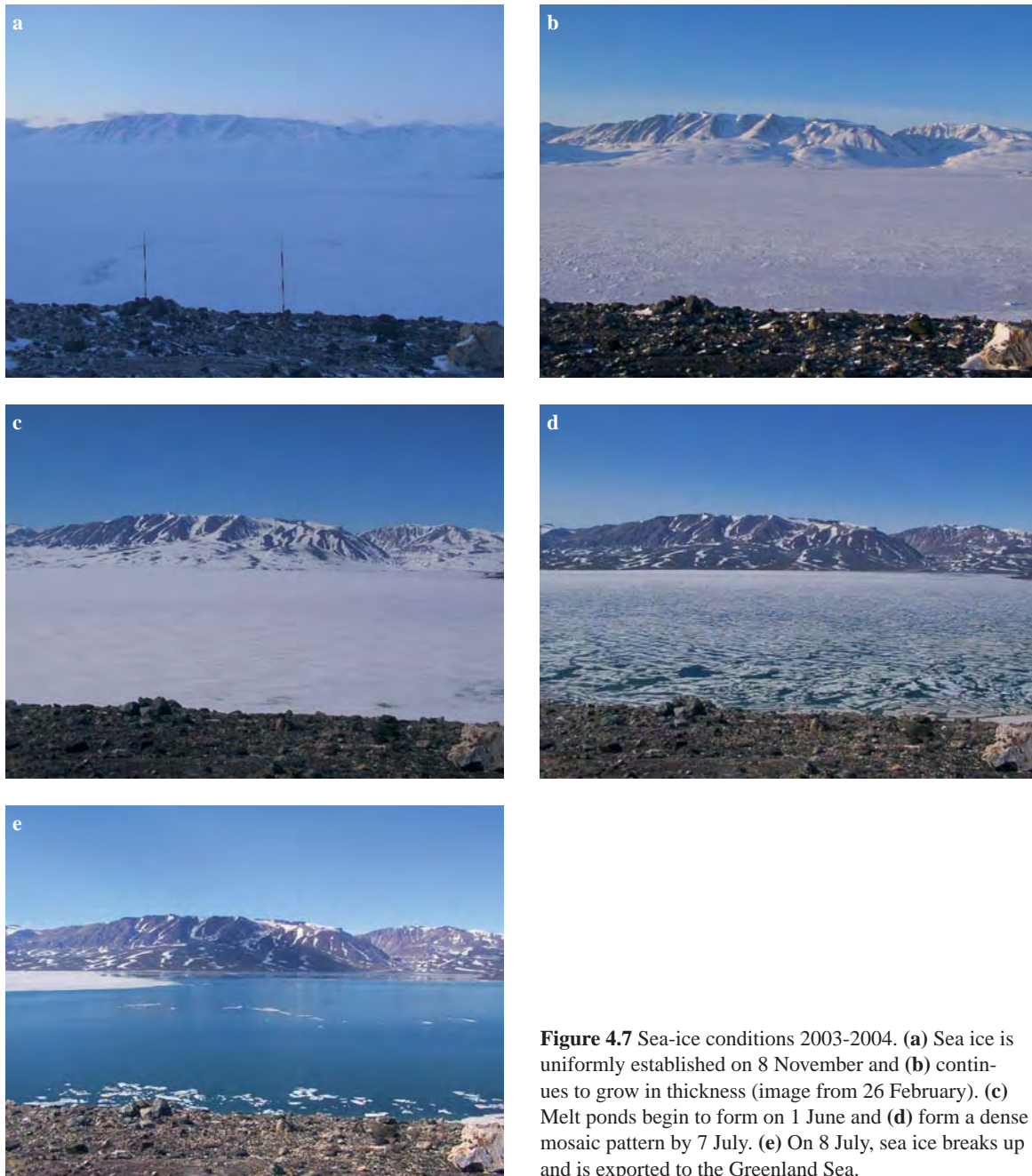
Figure 4.7 Sea-ice conditions 2003-2004. **(a)** Sea ice is uniformly established on 8 November and **(b)** continues to grow in thickness (image from 26 February). **(c)** Melt ponds begin to form on 1 June and **(d)** form a dense mosaic pattern by 7 July. **(e)** On 8 July, sea ice breaks up and is exported to the Greenland Sea.

Table 4.1 Irradiance reflectance of visible light from various types of snow and sea ice, as measured with a PAR (400–700 nm) quantum irradiance meter.

Medium	Irradiance reflectance $R_{(400–700\ nm)}$
Dry snow	0.73
Water-saturated snow	0.53
Slush ice	0.44
2 cm of water on ice	0.50
10 cm of water on ice	0.48
Sea water	0.18

a broadband PAR (400–700 nm) quantum irradiance meter (LiCor, USA) and with a spectroradiometer (FieldSpec® Analytical Spectral Devices, INC) – 380–1050 nm) during 7 June–5 July 1999. Unless otherwise indicated, all measurements were obtained under a clear sky around noon.

Early in June 1999, the sea ice was covered by a 20-100 cm thick layer of dry snow, and the irradiance reflectance, R, i.e. the ratio between the upwelling and downwelling irradiance, for the visible spectrum (PAR,

400–700 nm) amounted to 0.70–0.75 (Fig. 4.6a). Most of the incident light was thus reflected during this period. The reflectance values for NIR light (700–1050 nm) were, however, significantly lower and ranged between 0.35 and 0.50 due to the intrinsic absorption of red and NIR light in the ice-water matrix.

Later in the season the sea-ice surface turned into a mosaic of melt ponds and areas with more or less meltwater-saturated snow cover. On 29 June, we measured the irradiance reflectance in a number of spots representing different progression stages in snow-cover melt. In areas with dry snow, the situation was unchanged, while R (400–700 nm) had decreased to an average of 0.53 for wet snow, and in areas with slush ice or overlying water, the reflectance was even lower (0.48–0.40) (Fig. 4.6b). The reflectance from seawater in the emerging sea-ice holes was only 0.18. The reflectance of NIR light generally showed the same pattern, but the decrease in reflectance in dry snow versus wet snow was more pronounced in the red (<600–700nm) and NIR (>700nm) regions due to efficient absorption by water in this spectral region.

The reflectance of irradiance and the light propagation in snow is thus clearly affected by the water content. Dry snow contains a mixture of highly light-scattering snow crystals and air. The difference in refractive index between the two phases is relatively large, causing less forward scatter of the incident light. This increases the probability of incident photons being backscattered from the snow. As the water content increases, the difference in refractive index becomes less and scattering of the incident light thus becomes more forward biased (Perovich, 1996); a similar phenomenon is observed when sediments are wetted (Kühl & Jørgensen, 1994). Progressing snowmelt thus forms darker patches of more water-saturated snow on top of the sea ice (Fig. 4.7, see also Fig. 2 in Perovich, 1996 and Plate 3 in Perovich et al., 1998). The irradiance reflectance data is compiled in Table 4.1.

The high reflectance of snow causes strong light attenuation. Already below 4.5 cm of dry snow the downwelling irradiance of visible light was attenuated to <50% of the incident irradiance (Fig. 4.8). Below 24 cm of snow cover only 20–30% of the incident downwelling irradiance remained in the visible spectrum, while <5–10% of incident NIR remained. More detailed measurements of PAR transmission through snow and sea ice showed a strong exponential decrease of irradiance in the snow (Fig. 4.9) with
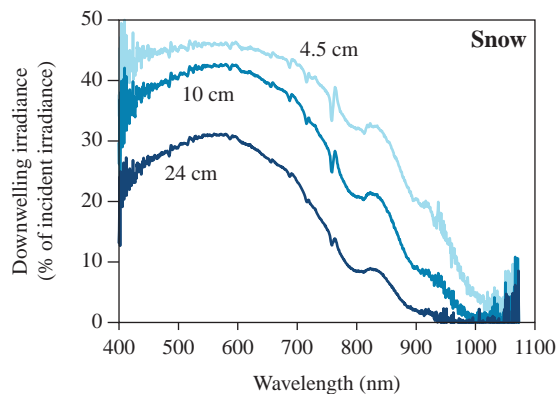
Figure 4.8 The spectral composition of the downwelling irradiance at three respective depths in dry snow.
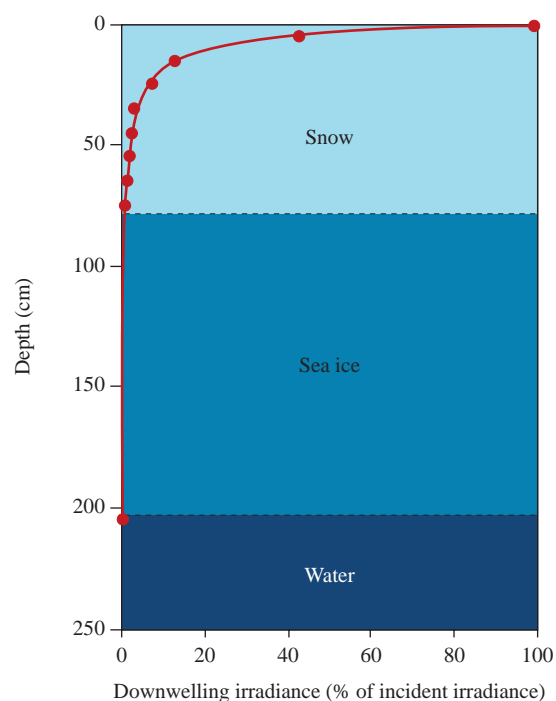
Figure 4.9 Downwelling irradiance profile (400–700 nm) through 75 cm of snow cover overlying 125 cm of sea ice.

an average attenuation coefficient of $K_{snow}= 5.6$ m^{-1}. However, closer inspection revealed that dry snow on top had a significantly higher light attenuation (9.5 m^{-1}), as compared to the lower layer of compressed snow at sub-zero temperature, which had an attenuation coefficient of about 1.5 m^{-1} (Fig. 4.10). The latter value was only slightly higher than in the underlying sea ice, which had an attenuation coefficient of about 0.9 m^{-1}. Attenuation coefficients in snow can vary from <4 to 40 m^{-1} and vary strongly with the water
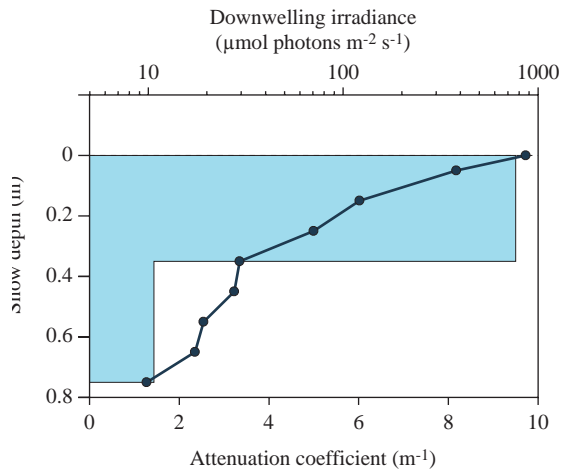
Figure 4.10 Downwelling irradiance (400–700 nm) though a 75 cm thick snow cover (from Fig. 4.6) reflecting two distinct light attenuation curves for the dry snow on top and the wet snow close to the sea ice.

content (Perovich, 1996). Perovich (1996) gives a range of 1.1–1.5 m⁻¹ for attenuation coefficients in sea ice. The actual value is, however, dependent on many environmental variables such as the temperature-dependent amount of brine inclusions in the ice and the amount of air bubbles and particulate material enclosed in the ice matrix. The higher attenuation in the top layer as compared to deeper layers in the ice seems to be a general observation in sea ice (e.g. Grenfell & Maykut, 1977).

Light intensity data loggers (Onset, HOBO) were placed at the water-ice interface by divers in order to obtain a continuous record of the visible light level below the sea ice. The data loggers were inter-calibrated with readings from a quantum irradiance sensor (LiCor, LI192) prior to deployments. The light levels clearly reflected a diurnal pattern with maximum values reaching 5–15 μmol photons m⁻² s⁻¹ (Fig. 4.11) around noon, corresponding to <0.1–1% of the incident downwelling irradiance, and virtually complete darkness at night due to the low sun angle during nighttime. There was a general trend of increasing light levels below the sea ice as the snow cover gradually melted (Fig. 4.11), and by the end of the melt the transmission of visible light had increased to 1–5% of the incident downwelling irradiance. The temporal variation in attenuation coefficient during the same measuring period was inferred from two simultaneous
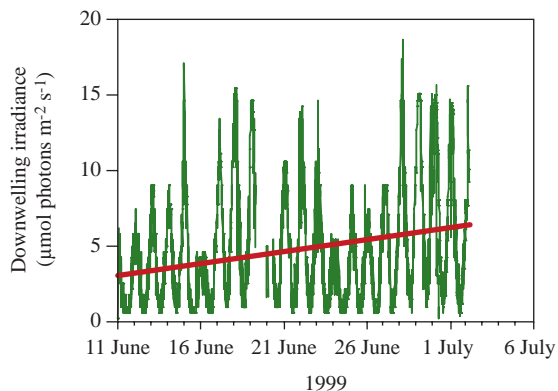
Figure 4.11 Downwelling irradiance measured below the sea ice during a 22-day period in 1999. The diurnal variation reflects the inclination of the sun as the period is characterized by midnight sun. Generally, the values showed an increasing trend towards the end of the measuring period as reflected by the linear approximation (red line), partly due to increased transparency of the ice cover and partly due to higher sun inclination. A few periods contain no data due to exchange of sensors.
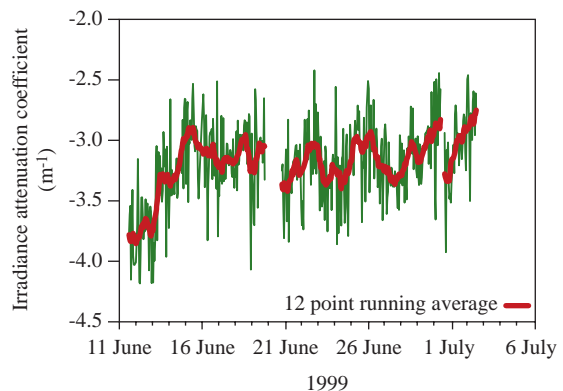
Figure 4.12 Light attenuation coefficient estimated from two continuous recordings of the light data loggers placed above and below the snow/sea-ice cover. The red line indicates a 12-point running average. The data reflects a gradual decrease in light attenuation.

recordings of light intensity loggers positioned above and below the snow/sea-ice cover, respectively (Fig. 4.12). The attenuation was highly variable but showed a decreasing trend during the first week, as the snow cover melted, and then reached a more or less stable value of c. 3.2 m^{-1} in the remaining period. The data only shows the conditions in one spot, but presumably reflects the general spring trend in Young Sound.

The spectral composition of the downwelling irradiance changed significantly during its passage through the snow and ice cover. Below the sea ice, mainly blue-green and yellow light (500–600 nm) prevailed, while blue and red light, as well as NIR light, was strongly attenuated due to the intrinsic absorption properties of water (data not shown). Very similar spectral transmission data was presented by Perovich et al. (1998) for relatively clean ice with no or very small amounts of particulate matter. The presence of particulate matter in ice will tend to decrease reflectance and increase attenuation of light. However, the ice in Young Sound generally was found to contain very low amounts of particles and only in a few cases was a distinct zone of dense material found in ice cores

Our data on reflectance and light transmission of sea ice in Young Sound is very similar to that reported in the literature on sea ice optics (e.g. Perovich, 1996). The temporal change in sea ice optical properties was studied in detail by Perovich et al. (1998) who observed similar decreases in reflectance and increasing light transmission during different stages of snow and ice melting. Our observations thus fit into the general pattern emerging from numerous studies of Arctic and Antarctic sea ice.

4.3.3 Sea-ice holes: Light effects and implications for primary production measurements.

It is generally accepted that in order to get realistic estimates of primary production it is important to incubate at *in situ* temperature and light conditions – preferably *in situ* (Clasby et al., 1973; Smith & Herman, 1991). In order to sample or access the bottom of the sea ice most studies require drilling of holes, and since sea-ice researchers often use standardized equipment, such ice holes tend to be of similar sizes, i.e. with diameters of 8–30 cm. For more elaborate sampling and SCUBA diving purposes larger holes of 80–150 cm in diameter are typical. It is also a common procedure to take advantage of the drilled hole and then place incubation flasks for O_2 exchange measurements or ^{14}C incuba-

tions within or at some distance from established holes to mimic *in situ* condition (e.g. Haecky & Andersson, 1999). Different strategies have been applied to reduce light artifacts near the hole, either by placing the bottles at different distances from the hole or covering the hole with various objects (Grossi et al., 1987; Hsiao, 1988). Furthermore, *in situ* profiling techniques adapted to work at different distances from the rim of sea-ice holes have been adapted (McMinn et al., 2000). However, no detailed studies have been published on light distribution around sea-ice holes or on the range and magnitude of light-induced artifacts.

In June 1998, a site with a homogeneous cover of c. 80 cm of dry snow was selected for studying light distribution and primary production activity around a diving hole in 150 cm thick sea ice. The amount of light passing through the snow cover was limited, and the scalar irradiance measured by a diver at the underside of the sea ice was only 0.3–1.5% of the incident downwelling irradiance (data not shown). A square hole of c. 1 m^2 was established without disturbing the snow cover on three sides of the hole. When the hole was established, the scalar irradiance was remapped. As expected, the irradiance immediately below the hole was significantly increased and at the rim (on the side with undisturbed snow cover) of the hole the underside of the ice now received c. 60% of the incident downwelling irradiance (Fig. 4.13a). As the incoming light also propagated horizontally in the snow and the sea-ice cover, a diffuse light field below the sea ice extended up to 8 m from the rim of the hole and reached a maximum water depth of 8 m at the rim. In this case, it was therefore necessary to perform any primary production incubations reflecting *in situ* conditions at least 8 m from the rim of the hole.

Water was sampled at selected depths and sea ice was collected from the bottom of the sea ice at least 8 m from the hole. ^{14}C incubations of water and sea-ice samples were performed in flasks placed at the respective depths. The light-limited primary production of sea-ice algae and phytoplankton in the upper part of the water column was significantly stimulated close to the hole (Fig. 4.13b). During two successive years with different snow cover thicknesses at the site of investigation (80 cm and 20 cm in 1998 and 1999, respectively), primary production of pelagic and sea-ice algae was investigated 4 times using parallel measurements at the center of and 8–10 m from two identical holes. Primary production in the upper 12

Downwelling irradiance (% of incident irradiance)

Primary production (µg C l⁻¹ d⁻¹)
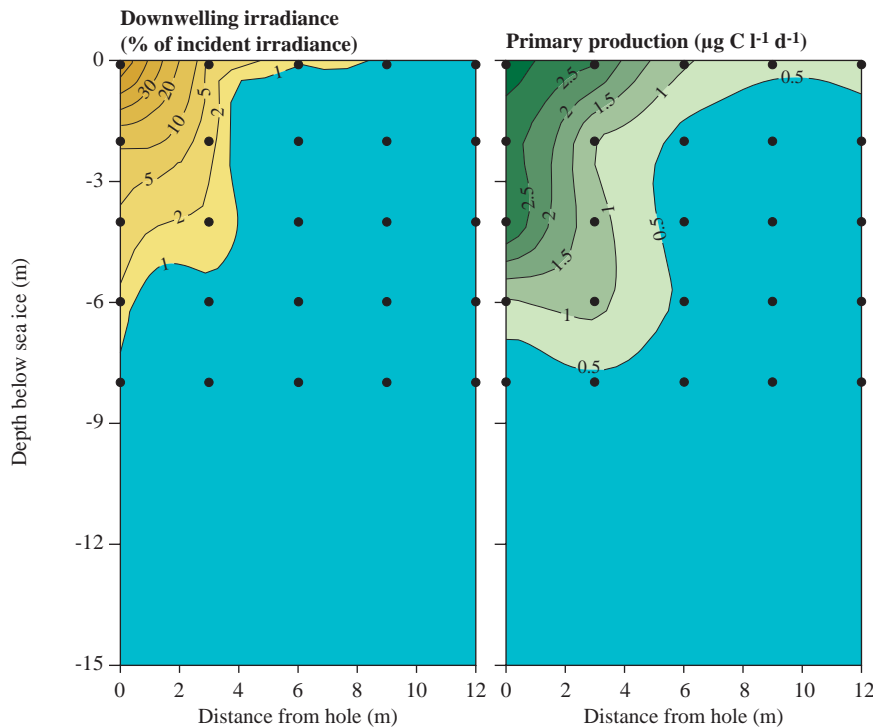
Figure 4.13 (a) Scalar irradiance relative to downwelling irradiance at the sea-ice surface as measured around the established diver hole (hole size c. 1 m²) and **(b)** primary production measured at the same positions. Zero "0" indicates the position of the ice edge and dots the points of actual measurements.
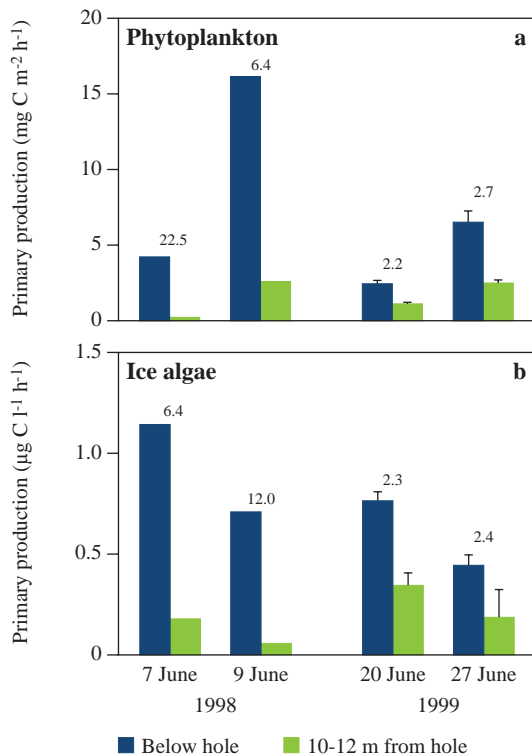
Figure 4.14 (a) Primary production measurements in water samples collected at 1 m depth and **(b)** in sea-ice samples collected at the underside of the ice as performed immediately below the hole and 10 m (or 12 m) from the edge of the sea-ice hole (hole size c. 1 m²). The values above the columns indicate the ratio between the two respective incubations.

m of the water column and the lower 0–4 cm of sea-ice was significantly overestimated when incubations were performed in the center of the hole compared with incubations performed at a distance of 10 m from the hole (Fig. 4.14). The strongest impact was observed in 1998, when snow cover was more extensive.

Our observations underline the importance of performing primary productivity measurements in and below sea ice at the correct *in situ* irradiance and show that the light conditions below or in the vicinity of a sea-ice hole can induce significant changes in the distribution and magnitude of productivity. The horizontal displacement of measuring equipment or incubation bottles required to avoid any light-induced artifacts due to sea-ice holes is dependent on many variables, including: Snow-cover thickness, ice thickness, the diameter of the hole, the sun angle and the optical properties of snow, ice and water. Predicting the light field below a sea-ice hole under given conditions is therefore not straightforward and nor is estimating where the incubation bottles should be placed to achieve correct *in situ* incubation. For a sea-ice hole with a diameter of c. 30 cm we measured an elevated scalar irradiance (>5%) up to 3 m from the hole (data not shown), and thus recommend that incubation bottles be placed at least 3 m from sea-ice holes for any measurements or incubations in the

given settings. As the light attenuation in sea ice is relatively small (see section 4.3.2) a simple routine for eliminating irradiance-induced artifacts in sea ice is to cover the sea-ice hole with a transparent Plexiglas plate and reestablish the overlying snow cover. Using non-transparent materials may reduce the light levels below the sea-ice hole. The presented data demonstrate how natural holes and cracks in the sea-ice or e.g. the edge of ice floes can represent sites with significantly elevated primary production.

4.3.4 Temperature, salinity, nutrient and oxygen dynamics of the sea ice during spring

The sea-ice temperature at Station A was recorded in 1999 and 2002. In both years the total ice thickness was practically unchanged during the study period, and the temperature and the shape of the profiles were very similar (only data from 2002 are presented). The temperature profiles reflect the heat exchange between sea-ice, air and water, respectively, leading to minimum temperatures in the central part of the ice cores (Fig. 4.15a). The minimum zone gradually migrated downward as the air temperature increased during spring/summer.

Measurements during the first half of June 2002 showed that both the brine salinity and the bulk salinity were elevated in the central part of the sea-ice core, and that the values decreased as the ice gradually melted (e.g. Fig. 4.15b). As a result, the calculated brine volume (Cox & Weeks, 1983) gradually increased and reached maximum values of 0.2–0.4 vol/vol at the sea ice/water interface at the end of the study period (Fig. 4.15c). The period was thus characterized by an almost linear increase in the tempera-
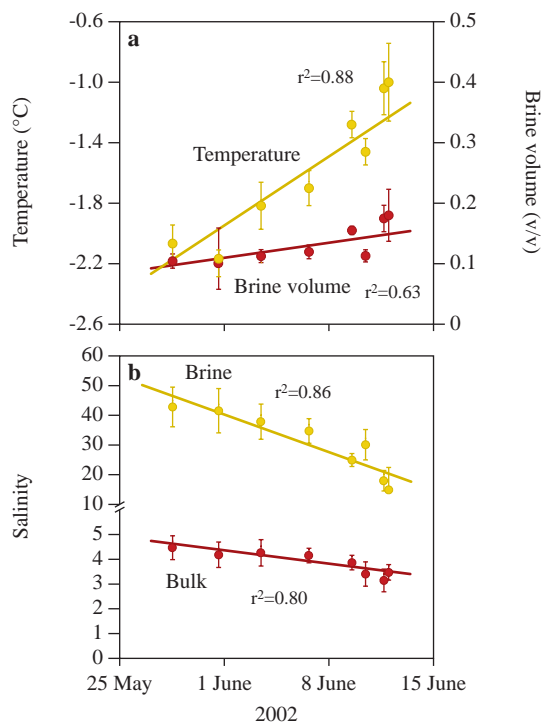
Figure 4.16 (a) Average temperature and brine volume during the study period of 2002 in the lower 0.5 m of the sea ice as derived from the values in Fig. 4.15. **(b)** The measured bulk salinity and the calculated brine salinity in the lower 0.5 m of the sea ice. Data from Rysgaard & Glud (2004).

Figure 4.15. Vertical profiles of temperature **(a)** and bulk salinity **(b)** measured from 28 May to 12 June during 2002. From these data, the brine volume at the respective depths was calculated and depicted in **(c)**. "0" depth indicates the position of the sea-ice/water interface. Data from Rysgaard & Glud (2004).
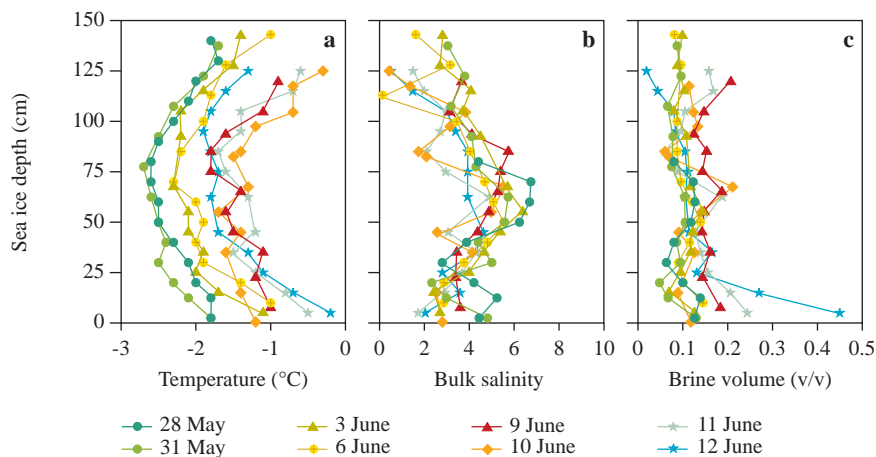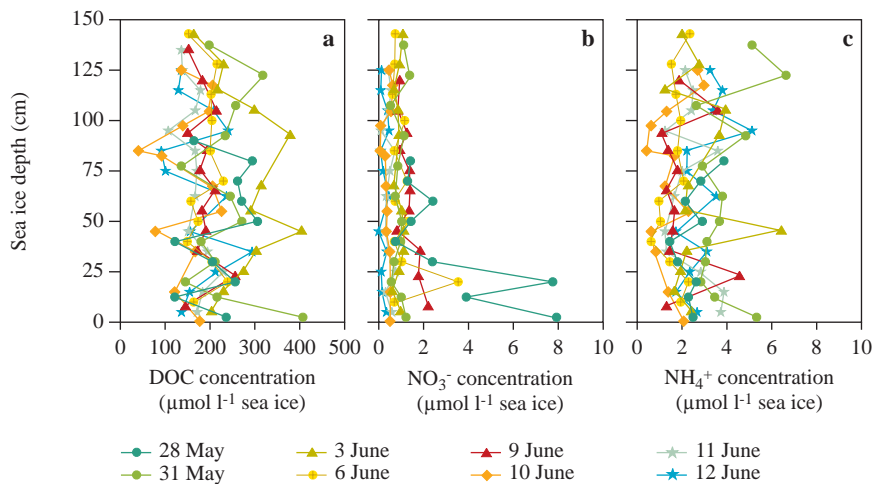
Figure 4.17 Selected vertical brine concentration profiles of DOC, NO_3^- and NH_4^+ (**a, b** and **c**) as measured during May-June 2002. Data from Rysgaard & Glud (2004).
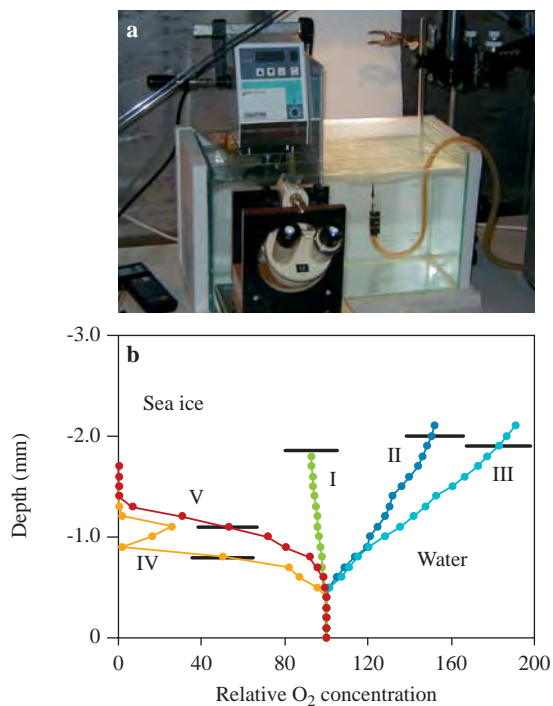
Figure 4.18 (a) A laboratory set-up, in which the temperature of air and seawater could be regulated independently. Thus, freezing of seawater and melting of sea ice could be closely regulated, while O_2 microprofile measurements were performed from below. **(b)** During sea ice formation (actively growing sea ice) O_2-enriched water was expelled from the sea-ice matrix, while meltwater leaving the receding sea-ice/water interface was O_2 depleted. The small horizontal lines indicate the position of the sea-ice/water interface for the individual O_2 microprofiles. Profiles were measured in the order I to IV as the sea ice grew in thickness (II and III) and subsequently receded (IV and V). Data from Glud et al. (2002).

ture and brine volume of the lower 0.5 m of sea ice (Fig. 4.16).

We intensively monitored the concentration of nutrients (NH_4^+, NO_3^-, PO_4^{3-}, Si) and DOC within the sea ice during the month of June in 1999 as well as in 2002. The concentrations and the shapes of the profiles were very similar during the two years (only data from 2002 are presented). The brine channels of the sea ice contained very high concentrations of DOC and relatively high concentrations of inorganic nitrogen (Fig. 4.17), while phosphorus and silicate concentrations in the brine were low (0.2–2.0 µM and 0.4–1.5 µM, respectively – data not shown). Apart from a weak tendency towards decreasing nutrient concentrations with time, there was no clear spatial or temporal pattern in the concentration profiles. All solutes were, however, present at all depths at all times. Recent studies have indicated that sea ice often contains very high concentrations of DOC (and POC) (Thomas et al., 2001; Krembs & Engel, 2001), and that a substantial fraction of this material consists of exopolymeric substances (EPS), produced by microorganisms in the brine channels under extreme conditions during the winter period (Krembs et al., 2002). EPS probably has a cryo-protective role and represents a previously overlooked source of organic carbon available for heterotrophic activity within sea ice.

While nutrient concentrations are standard parameters in many sea-ice studies, and their dynamics are well studied, the dynamics of gases in sea ice are much less investigated. Very recent studies have shown a high spatial and temporal variability in the O_2 concentration of sea-ice brine channels (Glud et

al., 2002; Mock et al., 2002). The O_2 concentration is obviously affected by photosynthesis and respiration (e.g. Gleitz et al., 1995; Günter et al., 1999) but is also highly sensitive to changes in temperature, salinity and, thus, brine volume. In sea ice without any biological activity, dissolved O_2 in principle behaves like other solutes; it accumulates in the brine as ice crystals form and only at extreme temperatures do the solutes freeze out with the developing crystals (Lappäranta & Manninen, 1988; Glud et al., 2002). The solute concentration of the brine thereby increases and becomes supersaturated with respect to O_2. As density gradients induce brine leakage from the developing sea ice, dissolved solutes and O_2 percolate out of the sea ice matrix and sink downwards (Glud et al., 2002). Conversely, when sea ice melts, O_2-depleted water is formed, and the brine now becomes undersaturated with respect to O_2 (and other gases) (Glud et al., 2002). Slight changes in air temperature around the freezing point of brine can thus lead to an oscillating leakage of supersaturated and undersaturated water from the sea-ice matrix (Fig. 4.18), potentially even on a diurnal scale. Biological activity inferred from O_2 measurements in sea ice should therefore be viewed with some reserve, especially during periods with oscillating air temperatures or during successive intervals of freezing and melting (Glud et al., 2002).

Dissolved gasses in freezing seawater can also establish bubbles. During late spring 0.5–8% of the sea ice in Young Sound consisted of gas bubbles, with a trend of increasing bubble volume towards the snow/ice interface (Fig. 4.19). This is presumably due to upward migration of bubbles in the constantly changing structure of the brine channel network. The total O_2 concentration of the sea ice exhibited a positive correlation with bubble volume, suggesting that a significant fraction of the O_2 was actually present in the gas bubbles (Fig. 4.20). However, simple mass-balance calculations revealed that both brine and gas bubbles were undersaturated with respect to O_2. Presumably, this was in part a result of ice melt, but heterotrophic microbial activity may also have contributed to the O_2 deficit (see below). The observations of a significant O_2 deficit in natural sea ice suggest potential existence of anoxic microniches and even associated anaerobic heterotrophic activity (Rysgaard & Glud, 2004).

Figure 4.19 Vertical profiles of the gas bubble volume and the total O_2 concentration in sea-ice cores from Young Sound in June 2002. The vertical dotted line in **(a)** indicates the expected gas volume at -1.8°C and a bulk salinity at 4, in **(b)** the line represents the atmospheric O_2 saturation at -1.8°C and a salinity of 33 (conditions at ice formation), respectively. Data from Rysgaard & Glud (2004).
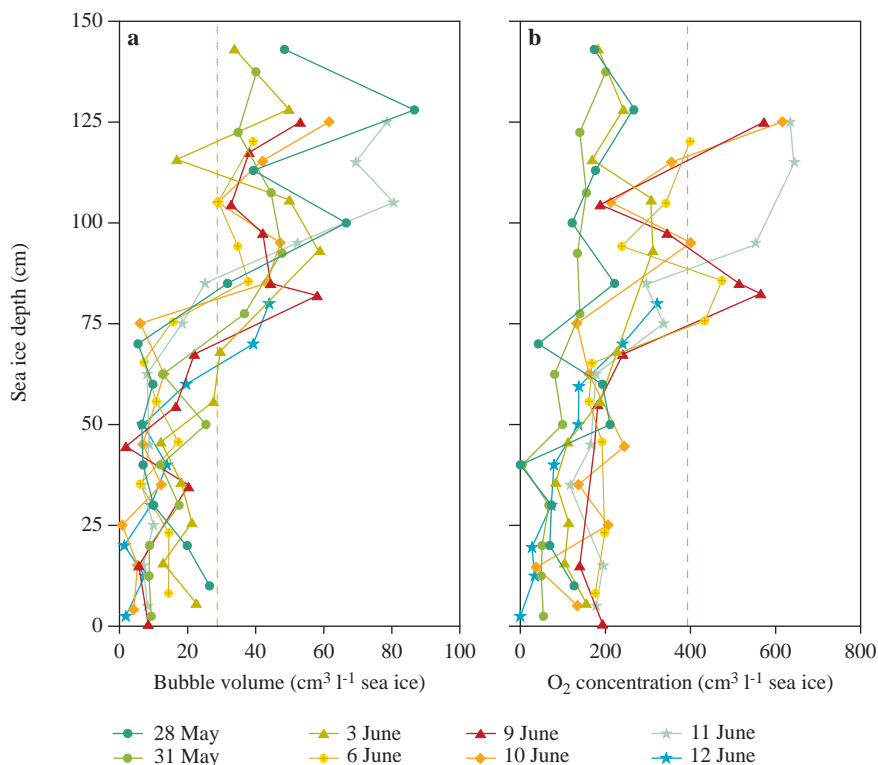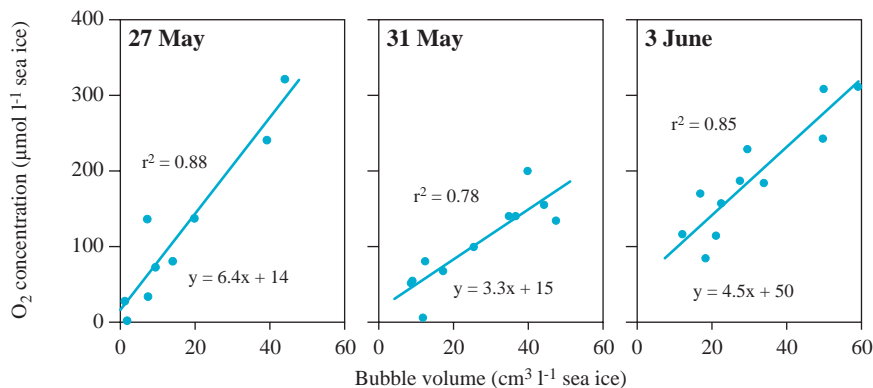
Figure 4.20 The total oxygen concentration of sea-ice sections as a function of the gas bubble volumes on three dates in 2002. Data from Rysgaard & Glud (2002).

4.3.5 Primary production of sea-ice algae in Young Sound

The importance of sea-ice algae for ecosystem carbon cycling has been addressed in various aquatic systems (Cota et al., 1991; Heckey & Andersson, 1999; Legendre et al., 1992; Arrigo, 2003). Especially in Antarctica, in the Canadian Arctic and along marginal ice zones, sea-ice-related primary production has been shown to add significantly to the ecosystem carbon production (Horner & Schrader, 1982; Palmisano & Sullivan, 1983; McMinn et al., 2000). Furthermore, it has been demonstrated that ice algae in receding ice covers may seed phytoplankton blooms and serve as an important food source for the planktonic grazers (e.g. Nelson et al., 1987; Michel et al., 1996).

In Young Sound, the dark winter (c. 3 months) and the open-water period (c. 3 months) restrict the period of potential sea-ice-related primary production to the remaining c. 6 months. Extensive snow cover on the sea ice may further narrow this period down
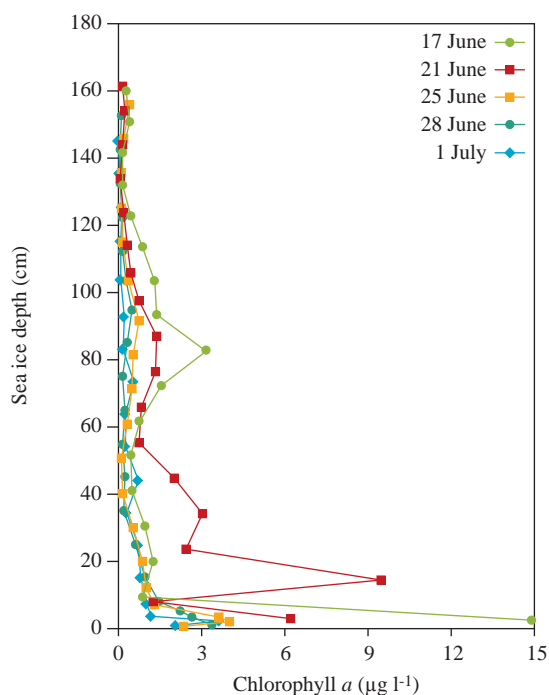
Figure 4.21 Vertical Chl *a* concentration profiles measured in sea-ice cores recovered from mid-June to early July 1999.
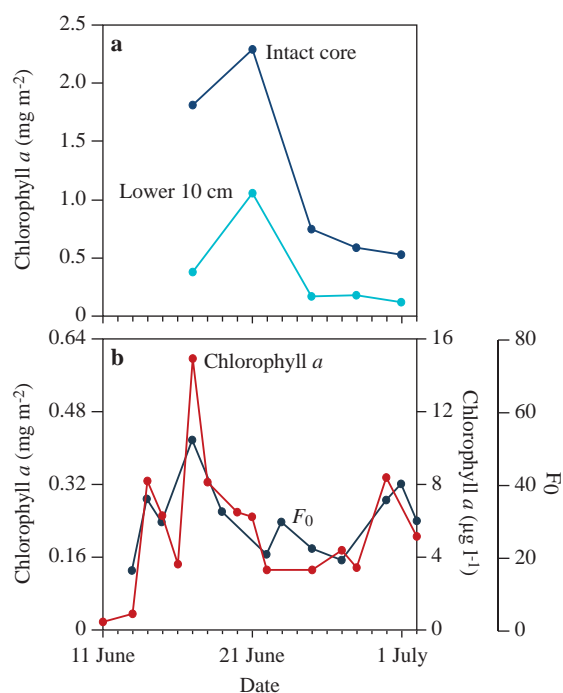
Figure 4.22 The Chl *a* concentration of intact sea-ice cores, **(a)** the lower 10 cm of the sea ice and **(b)** for the lower 4 cm of the sea ice. Panel **(b)** includes F_0 values obtained *in situ* by the diving PAM flourometer.

(see above). Sea-ice profiles of Chl *a* in Young Sound measured in June 1999 and June 2002 demonstrated that the phototrophic biomass was highest at the underside of the ice with maximum values of 9–15 µg Chl *a* l⁻¹ sea ice (Fig. 4.21). However, the Chl *a* content of the lower 10 cm represented only 20–40% of the value in intact sea-ice cores. The phototrophic biomass of both the lower 10 cm and of intact sea-ice cores reached a maximum in mid-June but then quickly decreased to a lower value, which remained constant for the rest of the month (Fig. 4.22a). A similar pattern in phototrophic biomass was found in 2002 (Rysgaard & Glud, 2004). Our depth-integrated sea-ice biomass of 0.5–2.5 mg Chl *a* m⁻² matches findings from open water in the Greenland Sea (Gradinger et al., 1999), but is significantly lower than the microalgal biomass reported from most other Arctic fast-ice areas, where values around 50–150 mg Chl *a* m⁻² are commonly reported (Arrigo, 2003).

The biomass profiles of intact sea-ice cores were complemented with more frequently obtained Chl *a* measurements in the lower 0–4 cm of the sea ice and by *in situ* PAM fluorometric determinations of the minimum chlorophyll fluorescence yield (F_0), which can be used as a proxy for the phototrophic biomass (see section 4.2.3). These measurements revealed very low values of phototrophic biomass during early June (before the first intact sea-ice profiles were made), but then showed an increasing trend, reaching a peak value in mid-June. The phototrophic biomass subsequently decreased but reached a second peak at the beginning of July (Fig. 4.22b). The PAM-derived dynamics in biomass correlated well with fluctuations in absolute pigment concentrations observed in the lower 4 cm of sea ice (Fig. 4.22b).

On 23 June 1999, more than 600 recordings of the F_0 values were obtained within an area of approximately 12×450 m. Measurements were separated by different horizontal distances from 1 cm to 450 m, and the calibrated values (see section 4.2.3) varied between 0 and 32.5 µg Chl *a* l⁻¹ in the lower cm of the sea ice (Fig. 4.23). Simple averaging yielded a phototrophic biomass of 4.2 ± 2.9 µg Chl *a* l⁻¹ at the underside of the ice, very similar to values obtained from direct quantification via collected sea-ice samples (3.2–4.0 µg Chl *a* l⁻¹; Fig. 4.22). Detailed statis-

Figure 4.23 Spatial variability in the F value (a proxy for the sea-ice related phototrophic biomass) quantified from 600 individual measurements obtained on 23 June 1999. Panels **(a)**, **(b)** and **(c)** show selected areas of Panel **(d)**. Data from Rysgaard et al. (2001).
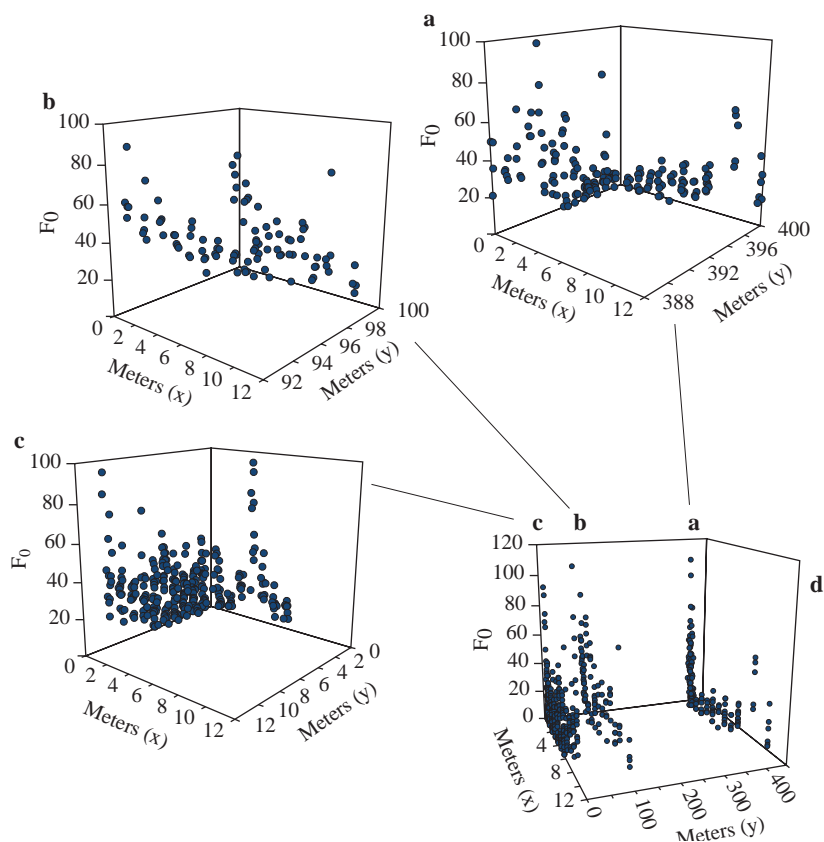
Table 4.2 Dominant diatom species at the water/sea-ice interface in Young Sound June 1999.

Chaetoceros affinis
C. socialis var. radians
Coscinodiscus cf. granii
Entomoneis alata
Fragilariopsis cylindrus
Melosira arctica
Navicula pelagica
N. vanhoeffenii
Nitzschia frigida
N. closterium
Porosira glacialis
Thalassiosira antarctica var. borealis
T. hyalina
T. nordenskioeldi

Figure 4.24 Three selected *in situ* O_2 microprofiles obtained at the sea-ice/water interface at a downwelling irradiance of 2–5 µmol photons m^{-2} s^{-1}. The profiles reflect elevated O_2 concentrations in the vicinity of the sea-ice surface. Data from Kühl et al. (2001).

tical analysis revealed that the biomass varied on a characteristic spatial scale of 5–10 m. In other words, patches of sea-ice algae had a characteristic diameter around 5–10 m (Rysgaard et al., 2001). This size matched the typical size of the melt ponds developing on the sea-ice surface during the initial stages of snow melt, and presumably reflects how light availability at the underside of the ice controlled the spatial distribution of the phototrophic biomass in the early stages of snow melt.

We did not perform any detailed taxonomic investigations, and simple microscopic investigations performed on directly melted ice cores do not provide a trustworthy quantitative diversity analysis (Gradinger, 1999). However, microscopic inspections of melted samples in June 1999 revealed that diatoms dominated the sea-ice-algal community. Dinoflagellates (mainly thecate types) were also encountered, but represented only a minor fraction of the total algal biomass. Eleven different diatom genera were observed and the most frequently observed species are listed in Table 4.2.

In situ microprofiling from the underside of the sea ice showed that during daytime the lower mm of the sea-ice occasionally became supersaturated with O_2 (Fig. 4.24). This could be interpreted as active photosynthesis. However, replicate microprofiling revealed an extreme spatial and temporal variability at the µm-scale and often O_2 microprofiles indicated a net heterotrophic community. Due to poorly defined transport coefficients within the sea-ice matrix, ice
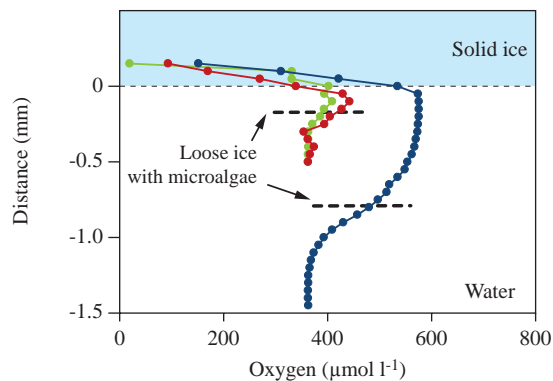
melt at the sensor tip (due to accelerated flow) and poor control on physically induced changes in O_2 concentrations (see section 4.3.4 and Glud et al., 2002), it was impossible to quantify photosynthetic activity from such profiles (Kühl et al., 2001; Glud et al., 2002). Photosynthetic activity of sea-ice algae has previously been inferred from *in situ* O_2 microprofiles that were, however, obtained in less dynamic environments with significantly higher phototrophic biomass, where the constraints we experienced apparently were of less importance (McMinn & Ashworth, 1998; McMinn et al., 2000). In the present study, we chose to infer gross photosynthetic activity of sea-ice-algal communities from ^{14}C incubations, as it is done in most other sea-ice studies.

In 1999, primary production was determined 10 times during a period of 22 days (11 June–2 July). On each sampling date, 10 cores were collected from the underside of the ice by divers, using a steel well 4 cm deep, with an area of c. 22 cm^2. The collected samples were pooled, homogenized and incubated in three replicate bottles around noon for 2 h at *in situ* light conditions. The data was converted to daily activities (24 h) taking into account the relative fraction of incoming irradiance during the incubation period in relation to total diurnal irradiance (Steeman-Nielsen, 1958). Primary production during the first 4 sampling dates was close to zero but positive signals were obtained for the rest of the sampling period, with peak values in mid-June and early July (Fig. 4.25a). Both peaks corresponded to increases

in phototrophic biomass (Fig. 4.22a). Integrated over the entire period (22 days) the values corresponded to a primary production of 5.3 mg C m^{-2}. However, this estimate only accounts for the lower 4 cm of the sea ice. At present, it is difficult to evaluate the extent to which Chl a found deep inside the sea-ice core actually represented photosynthetic active algae. However, measurements performed on interior sea ice sub-sampled from an intact sea-ice cores recovered on 1 July showed that the interior sea ice did contain active primary producers with an average activity of 5.7 µg C l^{-1}d^{-1} (n=3) at $in situ$ light conditions. Measurements by Mock & Gradinger (1999) also demonstrated that i) sea-ice algae encrusted deep inside the sea ice can be actively photosynthesizing and ii) that the integral interior primary production of 160 cm thick sea ice was similar to or even higher than the production in the bottom 5 cm. The Chl a-specific photosynthetic activity within each of two environments varied markedly (by a factor of 14) and, thus, Chl a-specific photosynthesis in the interior and in the bottom of the ice was not significantly different (Mock & Gradinger, 1999).

In 1999, the lower 4 cm of the sea ice studied here contained roughly 15% of the Chl a found in the entire sea-ice core. If we assume that the remaining Chl a represented phototrophic biomass with a specific primary production similar to that measured in the lowermost part of the sea ice, we achieve an estimate of total sea-ice-algal primary production during the study period of 35.9 mg C m^{-2} (or an average of 1.63 mg C m^{-2} d^{-1}). This estimate must be close to that year's annual contribution as the sea ice broke up on 10 July, i.e. 8 days after the end of the measuring campaign. As this estimate is extrapolated from the entire sea-ice core, it is somewhat higher than previously published estimates for Young Sound that accounted for only the lower 4 cm of the sea ice (Rysgaard et al., 2001; Glud et al., 2002). Extrapolating the values to the area of outer Young Sound (Region 1, 76 km^2 – see Chapter 3) the gross primary production amounted to only 2.7 t C. Even if the sea-ice-related activity during the 8 remaining days had been significant, the sea-ice-related primary production amounted to only <<1% of the total ecosystem production during 1999 (see Chapters 9 and 11).

In early June 2002, primary production in the lower 30 cm of sea ice was determined 5 times during a 6-day period using similar to that incubation pro-
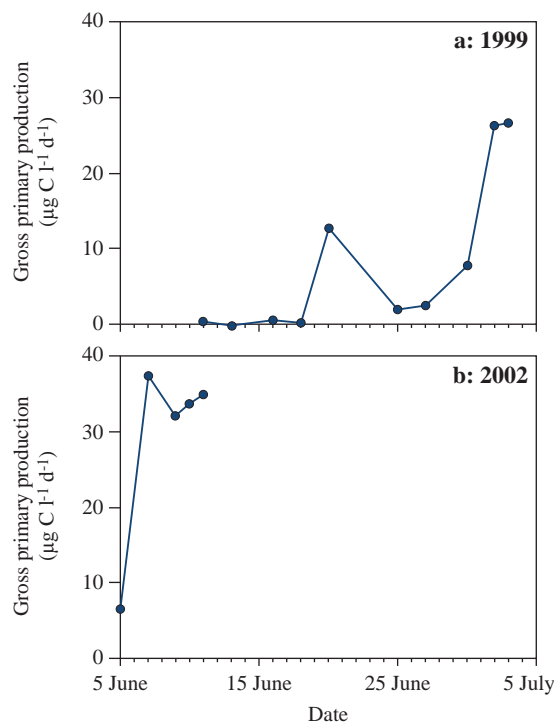
Figure 4.25 Values of sea-ice-related gross primary production measured during June **(a)** in the lower 4 cm of the sea-ice in 1999 and **(b)** in the lower 30 cm of the sea-ice in 2002.

cedure described above (Fig. 4.25b). That year had an exceptionally long open-water period (Fig. 4.5); the snow cover diminished and large melt ponds developed already in beginning of June, leading to increased light availability within the sea ice. The measured photosynthetic rates were thus somewhat higher than the corresponding values in 1999 (Fig. 4.24), yielding an integrated activity for the 6-day period of 55.2 mg C m^{-2} (in the lowermost 30 cm of the sea ice). Roughly 60% of the phototrophic biomass was present in the lower 30 cm of the sea-ice core during that period and the estimated activity for the entire sea-ice core thus amounted to 77 mg C m^{-2} (or an average of 12.8 mg C m^{-2} d^{-1}).

Sea-ice-related primary production in early June 2002 was thus significantly higher than in 1999, reflecting the interannual variations in light conditions and snow cover. Nevertheless, in both cases our values are in the lower end of most other fast-ice studies and not all of these accounted for the interior activity (Mock & Gradinger, 1999 and references therein). We speculate that the relatively thick snow cover and the extreme dynamics in the appearance
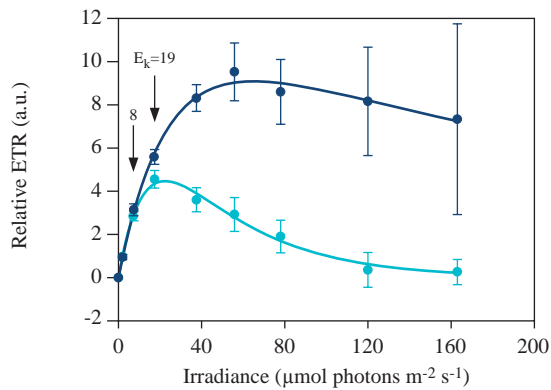
Figure 4.26 Relative ETR as a function of imposed light measured in two different sea-ice-algal communities growing at the rim of a sea-ice hole (dark blue) and 10 m from the hole (light blue). The ambient light levels during the investigation were 75 and 15 µmol photons m^{-2} s^{-1}, respectively. The light adaptation index, E_k, was calculated as $E_k = P_{max}/\alpha$, where P_{max} represents the maximum photosynthesis and α the initial slope of the light curve. Error bars indicate ± SD of 3–4 measurements. Data from Kühl et al. (2001).

and structure of the underside of the ice in Young Sound, which are strongly influenced by variations in freshwater input (see section 4.3.1), inhibit the establishment of larger sea-ice-algal communities in Young Sound.

The more traditional approach for estimating sea-ice-related primary production was complemented by PAM fluorometer-based measurements of sea-ice-algal activity (see section 4.2.3). Thereby, it was possible to resolve relations between light conditions and the relative photosynthetic ETR *in situ*, i.e. a proxy for the photosynthetic activity (see section 4.2.3.). The measurements showed that the sea-ice-algal community was well adapted to the ambient light levels. Communities growing in the vicinity of drilled holes and thus experiencing elevated light levels expressed a higher light adaptation index (E_k) and were only marginally photo-inhibited at 160 µmol photons m^{-2} s^{-1}, while communities growing more than 10 m from the holes were almost fully inhibited at this irradiance (Fig. 4.26). Likewise, communities underlying a developing melt pond gradually increased their light adaptation index from 12 to 35 µmol photons m^{-2} s^{-1} as the light levels below the sea ice increased (Fig. 4.27). The data clearly confirms that sea-ice-algal communities are very flexible and adapt quickly to changes in ambient light conditions (e.g. Lizotte & Sullivan, 1991).
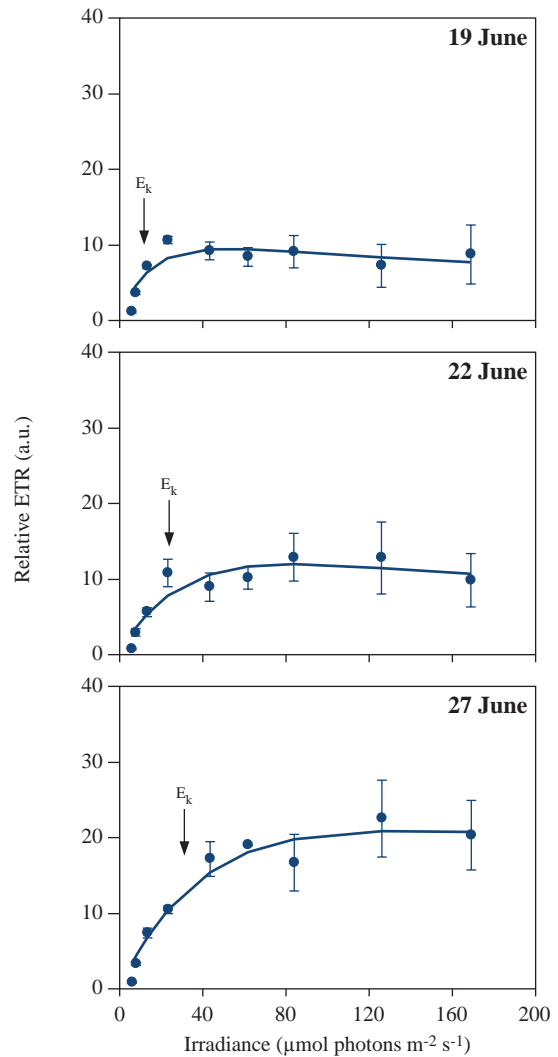
Figure 4.27 Relative ETR measured as a function of the imposed light at the same site on three different days. The E_k value of the sea-ice-algal community (calculated as $E_k = P_{max}/\alpha$) gradually increased from 12 to 35 µmol photons m^{-2} s^{-1} as the light availability below the sea ice increased. Data from Rysgaard et al. (2001).

Along with the 600 F_0 measurements recorded on 23 June 1999 we also recorded the effective quantum yield of PSII-related electron transport, ϕ_d (=ETR/ambient light) (see section 4.2.3). Statistical analysis showed that both ϕ_d and the irradiance below the sea ice expressed a characteristic spatial scale of variance of 50–100 m (Rysgaard et al., 2001). The data documented a spatial coupling between algal activity and light passing through the sea ice. Apparently the photosynthetic activity varied on a larger spatial scale than did the phototrophic biomass (see above). The lack of coupling between spatial variability of biomass and

activity could be related to differences in Chl *a*-specific activity induced by salinity variations. Another explanation could be a faster response in activity compared with biomass growth following changed light conditions as the melt pond grew in size (Rysgaard et al., 2001) or by inhomogeneous grazing patterns (Gradinger et al., 1992). Nevertheless, the data documents the close coupling between light availability and the activity of sea-ice-algal communities.

4.3.6 Heterotrophic activity of the sea ice

Sea ice contains high concentrations of POC and DOC, either i) entrapped during sea-ice formation, ii) resulting from phototrophic or heterotrophic growth within the sea ice or iii) transported into the sea ice by convective processes (Gradinger & Ikävalko, 1998; Weissenberger & Grossmann, 1998; Gradinger & Spindler, 1999). The carbon represents a potential food source for the bacterial community within the sea ice. Positive correlation has been demonstrated between the phototrophic and the heterotrophic prokaryotic biomass in some sea-ice habitats and this suggests a close metabolic coupling between the two communities (e.g. Gosink et al., 1993; Meiners et al., 2003). But other studies show no correlation between the abundances of the two communities, indicating that alternative carbon sources may also be of importance for the bacterial activity (e.g. Gradinger & Zang, 1997; Stewart & Fritsen, 2004). Recently, it was suggested that cryoprotective exopolymers of encrusted diatoms represent an important carbon source in Arctic winter sea ice (Krembs et al., 2002; Meiners et al., 2003).

Most studies on the importance of heterotrophic bacteria in sea ice have been based on simple enumeration, quantification of prokaryotic diversity or on culture work (Bowman et al., 1997; Mock et al., 1997; Huston et al., 2000; Junge et al., 2002). The lack of *in situ* data is due to the same experimental difficulties faced by scientists quantifying *in situ* photosynthetic activity (see above). The *in situ* microbial activity of sea ice has thus only been marginally explored.

During early June 2002 a number of ice cores were sampled at Station A. The lower 30 cm of each core was subsequently enclosed in water-containing gas-tight plastic bags, carefully avoiding entrapment of bubbles (Hansen et al., 2000; Rysgaard & Glud, 2004). The cores were then placed in the drilled holes and sampled at two-day intervals to determine the total O_2 concentration of the sea ice. In this way, the net aerobic activity of the enclosed sea-ice community was followed under *in situ* conditions. Surprisingly, the cores turned anoxic within 1 week due to a constant net O_2 consumption rate of 13 $\mu M\,O_2\,d^{-1}$ (Fig. 4.28). Given the concurrent photosynthetic activity measured in parallel ^{14}C incubations, corresponding to c. 2 $\mu mol\,O_2\,l^{-1}$ sea ice d^{-1} (Fig. 4.25b & Fig. 4.28), the gross heterotrophic activity thus amounted to c. 15 $\mu mol\,O_2\,l^{-1}\,d^{-1}$ (Rysgaard & Glud, 2004). This only accounts for the activity in the lower 30 cm of sea ice, but if we assume a similar specific rate for the rest of the sea-ice core, the O_2 consumption of the 160 cm thick sea ice of Young Sound amounted to c. 24 mmol $m^{-2}\,d^{-1}$ during the investigation period (Rysgaard & Glud, 2004). This corresponds to the oxygen uptake of dark-incubated sediment from 20 m water depth (Chapter 9) and is an extremely high activity, which cannot be representative of the ice cover of Young Sound during the entire ice-covered period as that would require a continuous supply of an unidentified carbon source. We thus refrain from extrapolating these findings, but the experiment documents that heterotrophic activity of sea ice can be substantial and that it can be of potential importance for ecosystem carbon cycling. The importance of heterotrophic activity in the sea ice of Young Sound is as poorly defined as in most other polar settings.

Even though advection and percolation of the sea-ice occur *in situ*, the high heterotrophic activity of the enclosed sea ice and the melting of O_2-depleted sea-ice crystals (see section 4.3.4) strongly suggest that anoxia
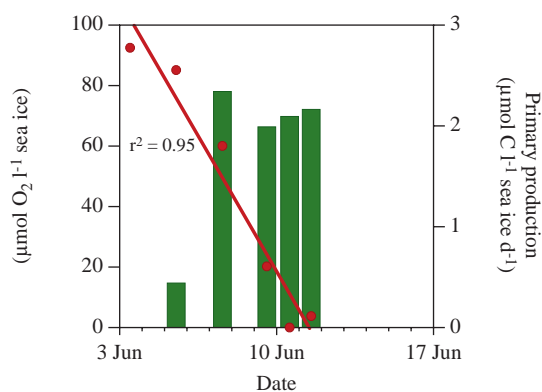
Figure 4.28 Primary production (green bars) and O_2 concentration (red line and symbols) in ice-core sections (bottom 30 cm) enclosed in a number of parallel gas-tight transparent incubation bags for a period of eight days. From Rysgaard & Glud (2004).

can develop in sea ice. This is supported by studies documenting the existence of purple anoxygenic phototrophic bacteria in Baltic sea ice (Petri & Imhoff, 2001) and the cultivation of denitrifying bacteria from sea-ice samples collected in Antarctica and in the Baltic Sea (Staley & Gosink, 1999; Kaartokallio, 2001). Sea ice collected in Young Sound did indeed host denitrifying bacteria in densities of 1.1×10^5 cells ml^{-1} sea ice, corresponding to 1.2×10^6 cells ml^{-1} brine (Rysgaard & Glud, 2004). Anoxic incubations of thawed sea-ice samples showed area-integrated denitrification rates of 10–45 µmol N m^{-2} d^{-1}, corresponding to 7–50% of the benthic denitrification activity (see Chapter 8). Thus, sea ice has a significant potential for acting as a sink in the nitrogen cycle. No sea-ice samples showed a potential for sulfate reduction, which could, however, be due to the relatively short incubation time of 24 h.

4.4   Synthesis and conclusions

Light availability is the major factor regulating the spatial distribution of biomass and activity of sea-ice algae. Before June, snow cover inhibits any significant sea-ice-related primary production in Young Sound, but as the snow becomes wet and melt ponds develop, light availability increases and the phototrophic biomass begins to flourish in the sea ice. Maximum levels of c. 15 µg Chl a l^{-1} were found at the underside of the ice, while the area-based ice-algal biomass reached a maximum value of c. 3 mg Chl a m^{-2} in mid-June. During a normal year, the melting of sea ice is accelerated during the second half of June and the interior as well as the underside of the sea ice become very dynamic habitats. Freshwater intrusions percolating through the sea-ice matrix combined with temperature fluctuations around 0°C change the sea-ice structure on a daily basis. Furthermore, the melting/freezing dynamics strongly affect salinity, nutrient and gas concentrations of the sea ice. These conditions make the sea ice in Young Sound a hostile environment, and we speculate that this is what prevents algae from colonizing the sea ice to the extent reported in other systems.

The main difference between Young Sound and most other fast-ice areas investigated is a massive snow accumulation on the ice surface during winter/early spring and a massive inflow of freshwater during the period of potential sea-ice-related primary production.

Snow cover and active sea-ice melt thus limit the time window of potential sea-ice-related primary production to around 1 month or less. In 1999, the annual gross production in the underside of the ice (0–4 cm) was estimated at 5.3 mg C m^{-2} yr^{-1}, while the value for the total sea ice was c. 36 mg C m^{-2} yr^{-1}. This is equivalent to only 2.7 t C for outer Young Sound (Region 1; Chapter 3). Interannual variations in sea-ice-algal production are to be expected, and extrapolation of the study in 1999 and the few measurements in 2002 should thus be done with caution. However, during the past decade of working in Young Sound we have never experienced any massive development of sea-ice algae.

Net production may be significantly smaller than inferred from the ^{14}C incubation procedure due to associated heterotrophic activity in the sea ice. Enclosure experiments on sea-ice cores during mid-June 2002 documented that the sea ice was net heterotrophic and thus did not represent a net source of organic carbon during that period. The annual heterotrophic activity of the sea ice in Young Sound is, however, poorly defined.

Microsensor and enclosure studies strongly indicated that anoxia can develop in sea ice, and tracer experiments documented that sea ice has a denitrification potential. The fact that sea ice can be net heterotrophic and can host anaerobic bacteria changes our present understanding of the role of sea ice in element cycling both quantitatively and conceptually.

4.5   Acknowledgements

4.6 References

Arrigo, K. 2003. Primary production of sea-ice. In: Sea Ice. Thomas, D.N. & Dieckmann, G.S., (eds.). Blackwell Science Ltd. 402 pp.

Braman, R. S. & Hendrix, S. A. 1989. Nanogram nitrite and nitrate determination inenvironmental and biological materials by Vanadium (III) reduction with chemiluminescence detection. Anal. Chem. 61: 2715-2718.

Bower, C. & Holm-Hansen, T. 1980. A salicylate-hypochlorite method for determining ammonia in seawater. Can. J. Fish. Aquat. Sci. 37: 794-798.

Bowman, J. P., Brown, M.V. & Nichols, D. S. 1997. Biodiversity and ecophysiology of bacteria associated with Antarctic sea ice. Antarct. Sci. 9: 134-142.

Clasby, R. C., Horner, R. & Alexander, V. 1973. An in situ method for measuring primary production of Arctic sea ice algae. J. Fish. Res. Board. Can. 30: 635-638.

Cota, G. F., Legendre, L., Grosselin, M. & Ingram, R. G. 1991. Ecology of bottom ice algae. I. Environmental controls and variability. J Mar Sys 2: 257-277.

Cox, G. F. N. & Weeks, W. F. 1983. Equations for determining the gas and brine volumes in sea-ice samples. J. Glaciol. 29: 306-316.

Eicken, H. 2003. From the microscopic, to the macroscopic, to the regional scale: Growth, Microstructure and Properties of sea Ice. In: Sea Ice. Thomas, D.N. & Dieckmann, G.S., (eds.). Blackwell Science Ltd. 402 pp.

Eicken, H., Bock, C., Wittig, R., Miller, H. & Poertner, H. O. 2000. Nuclear magnetic resonance imaging of sea ice pore fluids: methods and thermal evolution of pore microstructure. Cold Reg. Sci. Technol. 31: 207-225.

Giannelli, V., Thomas, D. N., Kennedy, H. A., Dieckmann, G. S., Kattner, G. & Haas, C. 2001. The behavior of dissolved organic matter during sea-ice formation, Ann. Glaciol. 33: 317-321.

Gleitz, M., Rutgers v. d. Loeff M., Thomas, D. N., Dieckmann, G. S. & Millero, F. J. 1995. Comparison of summer and winter inorganic carbon, oxygen and nutrient concentrations in Antarctic sea ice brine. Mar. Chem. 51: 81-91.

Glud, R. N., Gundersen, J. K. & Ramsing, N. B. 2000. Electrochemical and optical oxygen microsensors for *in situ* measurements. In: Buffle, J. & Horvai, G. (eds.), *In situ* analytical tecniques for water and sediment. John Wiley and Sons, Chichester: 19-75.

Glud, R. N., Rysgaard, S. & Kühl, M. 2002. A laboratory study on O_2 dynamics and photosynthesis in sea ice algal communities: Quantification by microsensors, O_2 exchange rates, ^{14}C-incubations and PAM fluorometry. Aquat. Microb. Ecol. 27: 301-311.

Golden, K. M., Ackley, S. F. & Lytle, V. I. 1998. The percolation phase transition in sea ice. Science 282: 2238-2241.

Gosink, J. J., Irgens, R. L. & Staley, J. T. 1993. Vertical distribution of bacteria in Arctic sea-ice. FEMS Microbiol. Ecol. 102: 85-90.

Gosselin, M., Levasseur, M., Wheelet P. A., Horner, R. A. & Booth, B. C. 1997. New measurements of phytoplankton and icealgae production in the Arctic Ocean. Deep-Sea Res. PII, 44: 1623-1643.

Gradinger, R. & Ikävalko, L. 1998. Organism incorporation into newly forming Arctic sea-ice in the Greenland Sea. J. Plank. Res. 20: 871-886.

Gradinger, R., Friedrich, C. & Spindler, C. F. M. 1999. Abundance, biomass and composition of sea-ice biota of the Greenland sea pack ice. Deep-sea Res. PII, 46: 1457-1472.

Gradinger, R. 1999. Vertical fine structure of the biomass and composition of algal communities in Arctic pack ice. Mar. Biol. 133: 745-754.

Gradinger, J.J. & Zhang, Q. 1997. Vertical distribution of bacteria in Arctic sea ice from Barents and Laptev Seas. Polar Biol 17: 448-454

Gradinger, R., Spindler, M. & Weissenberger, J. 1992. On the structure and development of Arctic pack ice communities in Fram Strait – a multivariate approach. Polar Biol. 12: 727-733

Grainger, E. H. & Mohammed, A. A. 1990. High salinity tolerance in sea-ice copepods. Ophelia 31: 177-185.

Grasshoff, K., Erhardt, M. & Kremling, K. 1983. Methods of seawater analysis. 2nd revised and extended version. Weinheim, Verlage Chemie, 419 pp.

Grossi, S. McG., Kottmeier, S. T., Moe, R. L., Taylor, G. T. & Sullivan, C.W. 1987. Sea ice microbial communities. VI. Growth and primary production in bottom ice under graded snow cover. Mar. Ecol. Prog. Ser. 35: 153-164.

Günter, S., Gleitz, M. & Dieckmann, G. S. 1999. Biogeochemistry of Antarctic sea ice: a case study on platelet ice layers at Drescher inlet, Weddell Sea. Mar. Ecol. Prog. Ser. 177: 1-13.

Haecky, P. & Andersson, A. 1999. Primary and bacterial production in sea ice in the northern Baltic Sea. Mar. Ecol. Prog. Ser. 20: 107-118.

Hansen, J. W., Thamdrup, B. & Jørgensen, B. B. 2000. Anoxic incubation of sediment in gas-tight plastic bags: A method for biogeochemical process studies. Mar. Ecol. Prog. Ser. 208: 273-282.

Hsiao, S. I. C. 1988. Spatial and seasonal variations in primary production of sea ice microalgae and phytoplankton in Frobisher Bay, Arctic Canada. Mar. Ecol. Prog. Ser. 44: 275-285.

Horner, R. A. & Schrader, G. C. 1982. Relative contribution of ice algae, phytoplankton, and benthic microalgae to primary production in nearshore regions of the Beaufort Sea. Arctic 35: 485-503.

Horner, R. A., Ackley, S. F., Dieckmann, G., Gulliksen, B., Hoshiai, T., Legendre, L., Melnikov, I. A., Reeburgh, W. S., Spindler, M. & Sullivan, C. W. 1992 . Ecology of sea-ice biota. 1. Habitat, terminology, and methodology. Polar Biol. 12: 417-427.

Huston, A. L., Krieger-Brockett, B. B. & Deming, J. W. 2000. Remarkably low temperature optima for extracellular enzyme activity from Arctic bacteria and sea-ice. Environ. Microbiol. 2: 383-388.

Jespersen, A. M. & Christoffersen, K. 1987. Measurements of Chlorophyll a from phytoplankton, using ethanol as extraction solvent. Arch. Hydrobiol. 109: 445-454.

Junge, K., Imhoff, F., Staley, T. & Deming, J. W. 2002. Phylogenetic diversity of numerically important Arctic sea-ice bacteria cultured at subzero temperature. Microb. Ecol. 43: 315-328.

Kaartokallio, H. 2001. Evidence for active microbial nitrogen transformation in sea ice (Gulf of Bothnia, Baltic Sea) in midwinter. Polar Biol. 24: 21-28.

Krembs, C. & Engel, A. 2001. Abundance and variability of microorganisms and transparent exopolymer particles across the ice-water interface of melting first-year sea ice in the Laptev Sea (Arctic). Mar. Biol. 138: 173-185.

Krembs, C., Eicken, H., Junge K. & Deming. 2002. High concentrations of exopolymeric substances in Arctic winter sea-ice: Implications of the polar ocean carbon cycle and cryoprotection of diatoms. Deep-Sea Res. PI, 49: 2163-2181.

Kühl, M. & Jørgensen, B. B. 1994. The light field of micro-benthic communities: radiance distribution and microscale optics of sandy coastal sediments. Limnol. Oceanogr. 39: 1368-1398.

Kühl, M., Glud, R. N., Borum, J., Roberts, R. & Rysgaard, S. 2001. Photosynthetic performance of surface associated algae below sea ice as measured with a pulse amplitude modulated (PAM) fluorometer and O_2 microsensors. Mar. Ecol. Prog. Ser. 223: 1-14.

Lappäranta, M. & Manninen, T. 1988. The brine and gas content of sea ice with attention to low salinities and high temperatures. Finnish Inst. Mar. Res. Internal Rep. 88-2.

Legendre, L., Ackley, S. F., Dieckmann, G. S., Gulliksen, B. & others. 1992. Ecology of sea-ice biota. 2. Global significance. Polar Biol. 12: 429-444.

Lizotte, M. P. & Sullivan, C. W. 1991. Rates of photoadaption in sea ice diatoms from McMurdo Sound, Antartica. J. Phycol. 27: 429-444.

McMinn, A. & Ashworth, C. 1998. The use of microelectrodes to determine the net production by Antarctic sea ice algae community. Antarct. Sci. 10: 39-44.

McMinn, A., Ashworth, C. & Ryan, K.-G. 2000. *In situ* net primary productivity of an Antarctic fast ice bottom algal community. Aquat. Microb. Ecol. 21: 177-185.

Meiners, K., Gradinger, R., Fehling, J., Civitarese, G. & Spindler, M. 2003. Vertical distribution of exopolymer particles in sea-ice of the Fram strait (Arctic) during autumn. Mar. Ecol. Prog. Ser. 248: 1-13.

Michel, C., Legendre, L., Ingram R. G., Gosselin, M. & Levasseur, M. 1996. Carbon budget of sea-ice algae in spring: evidence of a significant transfer to zooplankton grazers. J. Geophys. Res-Oceans. 101(C8): 18345-18360.

Mock, T., Meiners, K. M. & Giesenhagen, H. C. 1997. Bacteria in sea ice and underlying brackish water at 54 degrees 26'50''N (Baltic Sea, Kiel Bight). Mar. Ecol. Prog. Ser. 158: 23-40.

Mock, T. & Gradinger, R. 1999. Determination of Arctic ice algal production with a new *in situ* incubation technique. Mar. Ecol. Prog. Ser. 177: 15-26.

Mock, T., Dieckmann, G. S., Haas, C., Krell, A., Tison, J. L., Belem, A. L., Papadimitriou, S. & Thomas, D. N. 2002. Micro-optodes in sea ice: a new approach to investigate oxygen dynamics during sea-ice formation. Aquat. Microb. Ecol. 29: 297-306.

Nelson, D. M., Smith, W. O, Gordon, L. I. & Huber, B. A. 1987. Spring distribution of density nutrients and phytoplankton biomass in the ice edge zone of the Weddell-Scotia Sea. J. Geophys. Res. 92: 7181-7190.

Palmisano, A. C. & Sullivan, C. W. 1983. Sea ice microbial communities (SIMCO), 1. Distribution, abundance and primary production of microalgae in Mc. Murdo Sound, Antarctica in 1980. Polar Biol. 2: 171-177.

Perovich, D. K. 2003. Complex yet translucent: the optical properties of sea ice. Physica B 338: 107-114.

Perovich, D. K. 1996. The optical properties of sea ice, CRREL Monograph, 96-1, 25 pp.

Perovich, D. K., Roesler, C.S. & Pegau, W.S. 1998. Variability in sea ice optical properties, J. Geophys. Res. 103: 1193-1209.

Petri, R. & Imhoff, J. F. 2001. Genetic analysis of sea-ice bacterial communities in the Western Baltic Sea using an improved double gradient method. Polar Biol. 24: 252-257.

Revsbech, N. P. 1989. An oxygen microelectrode with a guard cathode. Limnol. Oceanogr. 34: 474-478.

Rysgaard, S., Nielsen, T. G. & Hansen, B. W. 1999. Seasonal variation in nutrients, pelagic primary production and grazing in a high-Arctic coastal marine ecosystem, Young Sound, Northeast Greenland. Mar. Ecol. Prog. Ser. 179: 13-25.

Rysgaard, S., Kühl, M., Glud, R. N., & Hansen, J. W. 2001. Biomass, production and horizontal patchiness of sea ice algae in a high-Arctic fjord (Young Sound, NE Greenland). Mar. Ecol. Prog. Ser. 223: 15-26.

Rysgaard, S. & Glud, R. N. 2004. Anaerobic N_2 production in Arctic sea-ice. Limnol. Oceanogr. 49: 86-94.

Schreiber, U., Hormann, H., Neubauer, C. & Klughammer, C. 1995. Assesment of photosystem II photochemical quantum yield by chlorophyll fluorescence quenching analysis. Aust. J. Plant. Physiol. 22: 209-220.

Schreiber, U., Schliwa, U. & Bilger, W. 1986. Continuous recording of photochemical and non-photochemical chlorophyll fluorescence quenching with a new type of modulation fluorometer. Photosynth. Res. 10: 51-62.

Smith, R. E. H. & Herman, A.W. 1991. Productivity of sea ice algae: *In situ* vs. incubator methods. J. Mar. Syst. 2: 97-110.

Staley, J. T. & Gosink, J. J. 1999. Poles apart: Biodiversity and biogeography of sea ice bacteria. Ann. Rev. Microbiol. 53: 189-215.

Steenmann-Nielsen, E. 1958. A survey of recent Danish measurements of the organic productivity in the sea. Rapp. PV Réun. Cons. Perm. Int. Explor. Mer. 144: 92-95.

Stewart, F. J. & Fritsen, C.H. 2004. Bacteria-algae relationships in Antarctic sea ice. Antar Science 16: 143-156

Thomas, D. N., Kennedy, H., Kattner, G., Gerdes, D., Gough, C. & Dieckmann, G. S. 2001. Biogeochemistry of platelet ice: Its influence on particle flux under fast ice in the Weddell Sea, Antarctica. Polar Biol. 24: 486-496.

Weeks, W. F. & Ackley, S. F. 1986. The growth, structure and properties of sea-ice. In: Untersteiner, N. (ed), The geophysics of sea ice. Martinus Nijhoff Publishers Dordrecht (NATO ASI B146): 9-164.

Weissenberger, J., Dieckmann, G. S., Gradinger, R. & Spindler, M. 1992. Sea ice: A cast technique to examine and analyze brine pockets and channel structure. Limnol. Oceanogr. 37: 179-183.

Weissenberger, J. & Grossmann, S. 1998. Experimental formation of sea ice: Importance of water circulation and wave action for incorporation of phytoplankton and bacteria. Polar Biol. 20: 178-188.